2 Renormalization group, universality and scaling in dynamics of coupled map lattices

S. P. Kuznetsov

Russian Academy of Sciences

2.1 Introduction

The concepts of renormalization group (RG), universality and scaling were formed initially in quantum field theory and in phase transitions theory. Beginning with Feigenbaum's work, they were introduced into the analysis of nonlinear systems. Thanks to this approach essential progress was achieved in understanding the nature of transitions to chaos via period-doublings, intermittency and quasiperiodicity [1–4].

It seems reasonable that the RG approach would also be effective for such systems as coupled map lattices (CML) [5–12], which are constructed of blocks with the above-mentioned types of behaviour. The approach may be briefly described as follows. Having the evolution operator of a spatially extended system for a certain time interval, we can find the new evolution operator for some larger interval and undertake the renormalization of variables to make the new operator as close as possible to the old one. This is just the RG transformation. We can continue to repeat the process to obtain a sequence of rescaled evolution operators for increasing time intervals. It may be found that for some special set of system parameters, the evolution operator for large values of time becomes invariant under the RG transformation. In other words, it represents the fixed point of some operator RG equation. This is just the critical situation near which the universality and scaling are valid. The universality arises because the fixed-point operator is determined by the structure of RG rather than by the actual form of the initial evolution operator. Scaling properties depend on the spectrum of eigenvalues of RG transformation linearized near the fixed point. Each essential eigenvalue with modulus exceeding 1 is responsible for one essential parameter of the system and gives a scaling constant for some direction in parameter space.

Theory and applications of coupled map lattices. Edited by K. Kaneko

The development of the RG approach must lead to the foundation of a theory of critical phenomena for the class of spatially extended systems simulated by CML. This theory will define what classes of universality exist and what are the dynamical properties of each class. Thereby, the CMLs may be considered as the most convenient representatives of their universality classes, being valid not only for qualitative but also for quantitative description of complicated spatiotemporal dynamics. Let us turn now to a brief review of results achieved in this field.

The first questions that arise when we begin to deal with CML are: does there exist some universality of coupling terms, how many essential parameters are needed for its description, and what scaling properties are inherent in them? These questions were stated and solved for coupled period-doubling systems in [13, 14]. It was shown that any small coupling is fully characterized by two essential parameters responsible for inertial coupling (associated with scaling factor $\alpha = -2.5029$) and dissipative coupling (scaling factor 2). For coupled maps exhibiting intermittency and quasiperiodicity the essential types of coupling were revealed by Pikovsky and colleagues [15, 16].

The RG analysis for spatially extended lattices of period-doubling maps was developed in my papers [17, 18] and recently by Kook, Ling and Schmidt [19], where the scaling factors α and 2 were again found. Waller and Kapral [9] and Kapral [20] have mentioned and explained scaling with constant α for regions of stability of uniform states for one- and two-dimensional lattices with linear coupling (with our terminology, this is a case of dominating inertial coupling). This range will be termed *lattice scaling*.

The properties of universality and scaling in continuum limit for spatially extended systems with symmetric dissipative coupling (or *diffusion*) were considered in our works [10, 21, 22]. It was shown that they are connected with the existence of a fixed-point operator of RG transformation including rescaling of the spatial variable by a factor of $\sqrt{2}$. Renormalization group analysis and scaling properties for the case of the addition of a few other types of coupling were considered in [23]. This range will be termed as continuous scaling.

Scaling with renormalization of spatial variable by $\sqrt{2}$ was also found by Kaspar and Shuster [24] for a chain of piecewise linear maps and by Bohr and Christensen [25] in numerical calculations with the two-dimensional lattice of period-doubling maps. Observation of scaling in a structure generated by the spatial return map for CML with diffusive coupling under random initial conditions was made by Crutchfield and Kaneko [7].

Aranson, Gaponov-Grekhov and Rabinovich have developed RG analysis for lattice systems with unidirectional coupling [26]. A new type of critical behaviour with non-Feigenbaum constants (bicriticality) was found in [27], and corresponding RG analysis was developed in [28].

In this chapter, consideration will be restricted to lattices of period-

doubling maps with mutual coupling, which is at present the best-studied class of CML. The structure of the chapter is as follows. Section 2.2 is devloted entirely to RG analysis. It begins with the simplest case of two coupled systems. Then the concepts of lattice and continuous scaling are introduced and the corresponding RG analysis is expounded. In Sections 2.3 and 2.4 the conclusions following from lattice and continuous scaling are considered and illustrated by a variety of computer results. In Section 2.5 the possibility of generalization to higher spatial dimensions is discussed and some computer illustrations for the two-dimensional case are presented.

2.2 Renormalization group analysis of one-dimensional coupled map lattices

2.2.1 *Two coupled period-doubling systems*

The central problem in the construction of CML is how to introduce a coupling between local maps. How does RG approach help us understand this problem? We start with the simplest case of two coupled elements. This plays a key role because the results obtained will allow us to build up easily to spatially extended lattices by including the pair interactions between neighbouring elements.

Thus, let us take the system of two identical symmetrically coupled maps

$$u_{l+1} = f_0(u_l, v_l),\ v_{l+1} = f_0(v_l, u_l), \tag{2.1}$$

where u, v are dynamical variables for subsystems and f_0 is a smooth function provided that the one-dimensional map $u_{l+1} = f_0(u_l, u_l)$ exhibits Feigenbaum's scenario of transition to chaos.

Let us express u_{l+2}, v_{l-2} in terms of u_l, v_l and make a change of variables $u \to u/a$, $v \to v/a$, where $a = -2.502907$ is Feigenbaum's scaling constant. This defines the RG transformation for f with transition to description of dynamics through doubling the time step. By using it over and over again, we obtain the recurrent equation

$$f_{n+1}(u, v) = a f_n((f_n(u/a, v/a)), f_n(v/a, u/a,)), \tag{2.2}$$

where f_n gives the form of the map similar to (2.1) for the evolution of u, v through 2^n iterations:

$$u_{l+2^n} = f_n(u_l, v_l),\ v_{l+2^n} = f_n(v_l, u_l).$$

Equation (2.2) has the fixed point

$$f(u, v) = g(u) \tag{2.3}$$

where $g(u)$ is Feigenbaum's universal function obtained as a solution of the equation $g(u) = ag(g(u/a))$ [1, 2].

Let us find a solution of (2.2) in linear approximation near the fixed point. Substituting $f_n(u, v) = g(u) + \varepsilon\varphi_n(u, v)$ we have

$$\varphi_{n+1}(u, v) = \hat{m}\varphi_n(u, v) \tag{2.4}$$

where the linear operator $\hat{m}$ is given by the relation

$$\hat{m}\varphi(u, v) = a[g'(g(u/a))\varphi(u/a, v/a) + \varphi(g(u/a), g(v/a))]. \tag{2.5}$$

For large n the solution of (2.4) will be a superposition of eigenfunctions of $\hat{m}$ having eigenvalues with modulus exceeding 1. Just as in the Feigenbaum theory, one must ignore the inessential eigenfunctions associated with infinitesimal changes of variables in the dynamical equation (2.1).

One class of eigenfunctions contains the functions that do not depend on the second argument. Of course, they correspond to perturbations of the fixed point (2.3) that do not include coupling. A unique essential of them is the function found by Feigenbaum [2]:

$$\begin{aligned}\Phi_0(u) = 1 &- 0.3256514\,u^2 - 0.0505539\,u^4 + 0.0145598\,u^6 \\ &- 0.0008810\,u^8 - 0.0001062\,u^{10} + 0.0000198\,u^{12},\end{aligned} \tag{2.6}$$

with eigenvalue $\delta = 4.669201$.

Another class contains the eigenfunctions that depend on both arguments and correspond to the introduction of coupling. By numerical solution of (2.4) one can find two such functions [13]:

$$\begin{aligned}\Phi_1(u, v) = {} & 0.6103456v - 0.0578582v^2 + 0.0000007v^3 - 0.004556v^4 \\ & + 0.0003007v^6 - 0.6103407u - 0.0000002uv \\ & - 0.000014uv^2 + 0.0000105uv^4 + 0.0578586u^2 \\ & - 0.0837668u^2v - 0.0208688u^2v^2 + 0.0000097u^2v^3 \\ & + 0.0005982u^2v^4 + 0.0000109u^2v^6 + 0.0837517u^3 \\ & + 0.000011u^3v^2 - 0.0000101u^3v^4 + 0.0254254u^4 \\ & - 0.0320244u^4v + 0.0019749u^4v^2 - 0.0000097u^4v^3 \\ & - 0.000095u^4v^4 + 0.032048u^5 - 0.0028781u^6 \\ & + 0.0057259u^6v - 0.0000446u^6v - 0.0057469u^7 \\ & + 0.0001322u^8 - 0.0002811u^8v + 0.0002906u^9,\end{aligned} \tag{2.7}$$

with eigenvalue $v_1 = a = -2.502907$; and

$$\begin{aligned}\Phi_2(u, y) = {} & -1.0586844v^2 + 0.0547721v^4 + 0.004464v^6 \\ & - 0.0005518v^8 + 1.0586824u^2 + 0.0357628u^2v^2 \\ & + 0.003456u^2v^4 - 0.0001064u^2v^6 - 0.0905175u^4 \\ & + 0.0351256u^4v^2 - 0.0010823u^4v^4 - 0.0430980u^6 \\ & - 0.0050244u^6v^2 + 0.0001013u^6v^4 + 0.0068283u^8 \\ & + 0.0001738u^8v^2 - 0.0003016u^{10},\end{aligned} \tag{2.8}$$

with eigenvalue $v_2 = 2$. It may be found that there are no additional essential eigenfunctions [13, 18, 19].

Now, we can write the explicit relation for the evolution operator for large n. The corresponding function f_n is

$$f_n(u,v) = g(u) + \varepsilon[\Lambda\delta^n\Phi_0(u) + C_1a^n\Phi_1(u,v) + C_2 2^n\Phi_2(u,v)]. \quad (2.9)$$

This representation is valid, of course, for sufficiently small deflection from the fixed point (2.3). However, it involves the following more general important conclusion.

One can see that for any initial map close to the RG fixed point (2.3) the asymptotic form of functions f_n as well as large temporal scale dynamics of the system will be governed by three parameters Λ, C_1, C_2. So, the structure of regions of different dynamical behaviour in the space of these parameters is universal. This structure also has a scaling property because the function f_{n+1} has at the point $(\Lambda/\delta, C_1/a, C_2/2)$ the same form that the function f_n has at the point (Λ, C_1, C_2). At both points the system demonstrates similar regimes with characteristic scale ratios equal to 2 for the time and a for the dynamical variables.

It is clear that Λ corresponds to deflection of the control parameter of individual maps from the critical point of accumulation of period-doubling bifurcations, while C_1 and C_2 characterize a coupling. The existence of two types of coupling with different properties relating to RG transformation means that we should introduce some terminology. For reasons explained later we call the two types *inertial* and *dissipative* couplings, respectively.

Let us now describe the procedure allowing us to represent any weak coupling as a combination of these types. It is based on a property of long-period cycles of the map (2.1) belonging to the invariant subspace $u = v$. By using the n-fold renormalized evolution operator $\{f_n(u,v), f_n(v,u)\}$ with $f_n(u,v)$ given by (2.9) the rescaled element of the period-2^n cycle is represented as the fixed point (u_*, u_*), where u_* is the root of the equation $u = g(u)$. We ask now: how do the multipliers of this cycle $\mu_n^{(1)}$, $\mu_n^{(2)}$ change in dependence on n? Calculating the eigenvalues of the derivative matrix for the map $\{f_n(u,v), f_n(v,u)\}$ at the point (u_*, u_*) we find

$$\mu_n^{(1)} = g'(u_*),\ \mu_n^{(2)} = g'(u_*) + \varepsilon[C_1D_1a^n + C_2D_2 2^n], \quad (2.10)$$

where $D_i = \frac{1}{2}[\partial\Phi_i(u,v)/\partial u]_{u,v=u_*}$. Multipliers $\mu_n^{(1)}$ and $\mu_n^{(2)}$ relate to symmetric and antisymmetric perturbations of the fixed point, respectively.

Thus, for analysis of the 'composition' of coupling in a given system of coupled maps it is necessary to find a sequence of (unstable) period-2^n cycles with $u = v$ at the point $\lambda = \lambda_0$ and calculate the derivatives of their multipliers $\kappa_n = (\partial\mu_n^{(2)}/\partial\varepsilon)_{\varepsilon=0}$. They must obey a relation $\kappa_n = C_1D_1a^n + C_2D_2 2^n$ and this allows us to find the coefficients C_1, C_2.

Let us take, for example, the system of a period-doubling map with linear coupling

$$u_{t+1} = f(u_t) + \varepsilon(u_t - v_t),\ v_{t+1} = f(v_t) + \varepsilon(v_t - u_t). \quad (2.11)$$

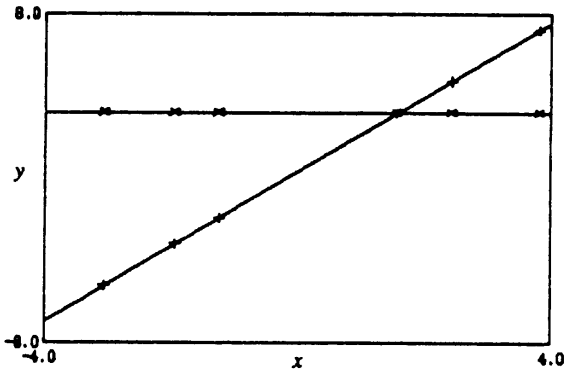

Figure 2.1 Plot for the estimation of coupling composition for the systems of two period doubling maps with linear (+) and quadratic (×) coupling.

Substituting $f(u) = \lambda - u^2$, $\lambda = \lambda_0 = 1.401155$ and performing the proposed calculations we present the results in Figure 2.1 using coordinates $X = (a/2)^n$, $Y = \kappa_n 2^{-n}$. According to the above argument, the point lie on the straight line $Y = C_1D_1X + C_2D_2$ and we find from the plot that $C_1D_1 = 1.821$ and $C_2D_2 = 0.281$. So, in this case we have the combination of inertial and dissipative coupling with the former dominating.

The system with quadratic coupling

$$u_{t+1} = f(u_t) + \varepsilon(f(v_t) - f(u_t)),\ v_{t+1} = f(v_t) + \varepsilon(f(u_t) - f(v_t)), \quad (2.12)$$

may also be presented in an equivalent form of future coupling

$$u_{t+1} = f(u_t) + \varepsilon'(v_{t+1} - u_{t+1}),\ v_{t+1} = f(v_t) + \varepsilon'(u_{t+1} - v_{t+1}), \quad (2.13)$$

where $\varepsilon' = \varepsilon/(1 - 2\varepsilon)$. In both these cases we find by the same argument $C_1D_1 = 0$ and $C_2D_2 = 3.202$ (see Fig. 2.1). This coupling is fully dissipative.

Then arbitrary relation of inertial and dissipative coupling may be obtained by the combination of

$$u_{t+1} = f(u_t) + \varepsilon_1(u_t - v_t) + \varepsilon_2(f(v_t) - f(u_t)),$$
$$v_{t+1} = f(v_t) + \varepsilon_1(v_t - u_t) + \varepsilon_2(f(u_t) - f(v_t)). \quad (2.14)$$

This is a *universal model* of two weakly coupled symmetric period-doubling systems containing the full 'zoo' of phenomena exhibited by this class in a region of scaling. So, there is no necessity to study any other systems.

In particular, the pure inertial coupling may be realized by special selection of coefficients taking into account the data of Figure 2.1:

$$u_{t+1} = \lambda - u_t^2 + \varepsilon(1 - 0.176u_t)(u_t - v_t),$$
$$v_{t+1} = \lambda - v_t^2 + \varepsilon(1 - 0.176v_t)(v_t - u_t) \quad (2.15)$$

In conclusion we will explain the terminology. It is easy to see that the coupling in equations (2.12) tends to equalize the instantaneous states of subsystems (for $0 < \varepsilon < 1/2$). In fact, for any u, v the Jacobi determinant obeys the inequality $J(\varepsilon) = J(0) < (1 - 2\varepsilon) < J(0)$. This gives a basis for the term 'dissipative coupling'. On the other hand, due to coupling, the map (2.15) preserves the memory of the previous state (in the order of u, v) when the state passes near the origin. This justifies the term 'inertial coupling'.

2.2.2 *Long lattice, universal model and lattice scaling*

We now turn to consideration of extended one-dimensional CML. We require the translation invariance to hold and suppose initially that only the nearest neighbours are coupled.

The RG analysis is constructed as in the previous section. The fixed point of RG transformation is the set of uncoupled maps

$$\{\dots g(u_{m-1}), g(u_m), g(u_{m+1}) \dots\}, \tag{2.16}$$

where m is the spatial index.

Let us consider any small perturbation of the fixed point corresponding to the inclusion of coupling. For each cell we must take into account the action from the left and the right neighbours, which may be given, in general, by different functions $\varphi(u_m, u_{m-1})$ and $\psi(u_m, u_{m+1})$. (We assume here that $\varphi(u, u) = 0$, $\psi(u, u) = 0$.) For weak coupling both terms must be entered in the dynamical equation additively :

$$u_{l+1,m} = g(u_{l,m}) + \varepsilon[\varphi(u_{l,m}, u_{l,m-1}) + \psi(u_{l,m}, u_{l,m+1})]. \tag{2.17}$$

where l is the temporal index.

We can easily check that RG transformation for functions φ and ψ is obtained again in the form (2.4). For large n, each of these functions will turn into the linear combination of eigen functions Φ_1, Φ_2 (see (2.7), (2.8)). Corresponding coefficients A_1, A_2 (for φ) and B_1, B_2 (for ψ) will be the essential parameters of coupling. Furthermore, taking into account the eigenfunction Φ_0 responsible for perturbation of the control parameter, the following representation of the evolution operator through 2^n time steps may be written for the lattice in rescaled variables:

$$\begin{aligned} u_{l+2^n,m} = {} & g(u_{l,m}) + A\alpha^n[\phi_1(u_{l,m}, u_{l,m+1}) - \phi_1(u_{l,m}, u_{l,m-1})] \\ & + B2^n[\phi_2(u_{l,m}, u_{l,m+1}) - \phi_2(u_{l,m}, u_{l,m-1}) \\ & + C\alpha^n[\phi_1(u_{l,m}, u_{l,m+1}) - \phi_1(u_{l,m}, u_{l,m-1})] \\ & + D2^n[\phi_2(u_{l,m}, u_{l,m+1}) - \phi_2(u_{l,m}, u_{l,m-1}) + \Lambda\delta^n\phi_0(u_{l,m}). \end{aligned} \tag{2.18}$$

Here, $A = (A_1 - B_1)/2$, $B = (A_2 - B_2)/2$, $C = (A_1 + B_1)/2$, $D = (A_2 + B_2)/2$ are the parameters of antisymmetric inertial, antisymmetric dissipative,

symmetric inertial and symmetric dissipative coupling respectively. The next scaling property of CML follows from (2.18): similar dynamics will be realized at the points of parameter space $(\Lambda/\delta, A/a, B/2, C/a, D/2)$ and (Λ, A, B, C, D) with rescaling of u by a and doubling of the temporal scale in the first case. We call it the *lattice scaling*.

Using the models of two coupled systems discussed in Section 2.2.1, the lattices may be constructed easily with all types of coupling or with any one of them. The *universal model* with parameters suitable for RG analysis may be written in the form

$$\begin{aligned} u_{l+1,m} = {} & \lambda - u_{l,m}^2 + A(1 - 0.176u_{l,m})(u_{l,m+1} - u_{l,m-1}) \\ & + B(u_{l,m+1}^2 - u_{l,m-1}^2) \\ & + C(1 - 0,176u_{l,m})(u_{l,m+1} - 2u_{l,m} + u_{l,m-1}) \\ & - D(u_{l,m+1}^2 - 2u_{l,m}^2 + u_{l,m-1}^2). \end{aligned} \tag{2.19}$$

The terms of the dissipative coupling have a simple physical interpretation. The properties of a symmetric term just correspond to the *diffusion*, while the antisymmetric one provides the *transfer* of perturbations along the lattice.

The system with pure diffusion is an interesting caste. Most aspects of its dynamics have been studied in computer experiments and it is important for the further development of RG. The next section is devoted to this case.

2.2.3 *Lattices with diffusive coupling and renormalization-group fixed point in continuum limit*

For lattices with pure diffusion the revised version of RG may be assumed including proceeding to continuum limit and rescaling of the spatial coordinate. This leads to a somewhat more pragmatic type of scaling allowing us to compare the states of the spatially extended system without coupling parameter change. We shall now consider this case.

The CML with pure diffusion may be described by (2.19) with $A = B = C = D = 0$:

$$u_{l+1,m} = f(u_{l,m}) + D[f(u_{l,m-1}) - 2f(u_{l,m}) + f(u_{l,m+1})], \tag{2.20}$$

or by the future coupling equation for the lattice constructed on the base of blocks (2.13):

$$u_{l+1,m} = f(u_{l+1,m}) + D(u_{l+1,m-1} - 2u_{l+1,m} + u_{l+1,m+1}). \tag{2.21}$$

Let the local map parameter λ equal to Feigenbaum's critical value λ_0 and the coupling D be sufficiently small. Then, let us perform the RG procedure of Section 2.2.2 many times. At each new step we deal with the states of the lattice concentrated in smaller and smaller intervals of the dynamical variable ($u \sim 1/a^n$) while the effective coupling parameter increases as $D.2^n$.

For sufficiently large n the linear approximation (2.9) fails. However, it is quite reasonable to suppose that in this situation of extremely strong influence of dissipative coupling only patterns would arise that have a very small difference between the neighbouring cells. Returning to description of the situation by the initial dynamical equation, we can proceed to a continuous spatial variable x and replace the difference term by a derivative:

$$u_{t+1}(x) = f(u_t(x)) + D\frac{\partial^2}{\partial x^2} f(u_t(x)). \tag{2.22}$$

Now, rescaling the coupling parameter by 2 is equivalent to rescaling the spatial variable by $\sqrt{2}$. So we can redefine the RG transformation for it to have the fixed-point operator corresponding to a distributed coupled map medium with diffusion rather than to an uncoupled map lattice.

Let us consider this development of the approach in detail. Denoting the initial evolution operator by $G_0[u]$ we use this operator twice and make the scale change $\hat{S}u(x) = au(x\sqrt{2})$. Then the new operator $G_1[u] = \hat{S}G_0\hat{S}^{-1}[u]$ is obtained by evolution through two time steps. Repeating this many times, we come to the recurrent operator equation

$$G_{n+1}[u] = \hat{S}G_nG_n\hat{S}^{-1}[u], \tag{2.23}$$

where G_n is the renormalized evolution operator for 2^n steps. The following statements should be valid.

(1) Let the initial operator G_0 be the evolution operator of a spatially extended system constructed from period-doubling cells with diffusive coupling. Then for the critical value of the cell control parameter the sequence of operators generated by (2.23) converges to regular limit G. This operator is the fixed point of the RG equation

$$G[u] = \hat{S}GG\hat{S}^{-1}[u]. \tag{2.24}$$

(2) The operator G is universal, i.e. it is the same for all systems with diffusive coupling. The only difference may be in characteristic scales for u and x.

We notice that both models (2.20) and (2.21) admit factorization in the form

$$u_{t+1}(x) = \hat{L}f(u_t). \tag{2.25}$$

This is no accident. It may be shown that the possibility of such representation is a sufficient condition for the system to belong to the universality class associated with the fixed point G. For this class the map f would exhibit Feigenbaum's period-doublings and the linear operator must satisfy the following requirements:

(1) Translation invariance: the operator can be represented in general as $\hat{L}u_m = \sum C_j u_{m-j}$ for discrete systems or as $\hat{L}u(x) = \int C(\xi)u(x-\xi)\mathrm{d}\xi$ for continuous ones.

(2) Symmetry: $C_m = C_{-m}$ or $C(\xi) = C(-\xi)$.

(3) Normalization: $\sum C_m = 1$ or $\int C(\xi)\mathrm{d}\xi = 1$.

(4) Locality: the sum $d^2 = \sum m^2 C_m$ or the integral $d^2 = \int \xi^2 C(\xi)\mathrm{d}\xi$ is finite. The value d defines the characteristic spatial scale for operator $\hat{L}$—diffusion length per time step.

(5) Dissipativity: the spectrum $L(k) = e^{-ikx}\hat{L}e^{ikx}$ lies with in the unit circle ($|L(k)| < 1$, $k \neq 0$).

A mathematically rigorous proof for these statements will not be given here, but we shall demonstrate the convincing results of its numerical varification. For this, the following procedure was performed for several values of the number $k = 1, 2, \ldots 5$. We take the CML (2.21) containing M_k cells with periodic boundary conditions. Here $M_0 = 26$ is an arbitrarily chosen integer and M_k is the integer nearest to $2^{k-2}M_0$. Then, we take the ensemble of probe functions U_m as the linear combination of the several sinusoidal components having the wave numbers $2\pi/M$, $4\pi/M, \ldots$ with random amplitudes and phases. We also perform normalization such that $U_{\min} = -1$ and $U_{\max} = 1$. Then, we give the initial condition for (2.21) as $u_{0,m} = U_m a^{-k}$ and interate this equation 2^k times. The end states are shown in Figure 2.2a, b for two representatives of the ensemble $\{U_m\}$ in coordinates $X = m/M_k$, $Y = ua^k$. These are the plots of the functions $G_k[U_m]$ against the spatial variable. One can see an excellent convergence of the points for increasing k. The limit is just the result of action of the fixed-point operator G on the probe function $U_m(x)$.

In the same manner we can verify the universality. For this, the above scheme of calculations is reproduced for several different systems (2.25). Notice that the lengths of the systems must be chosen to make the value M/d equal in all the cases. Examples of such calculations are presented in Figure 2.2c, d for three systems. One can see that the configurations obtained for sufficiently large $k = 5$ coincide very well in full accordance with our hypothesis of universality.

2.2.4 *Universal model in continuum limit*

Following the logic of the RG approach, we must now turn to the analysis of solutions for the RG equation (2.23) near the fixed point G. Substituting $G_n[u] = G[u] + \varepsilon h_n[u]$ into (2.23) and supposing $\varepsilon \ll 1$, we obtain the operator equation

$$h_{n+1}[u] = \hat{S}G'(G\hat{S}^{-1}[u])h_n\hat{S}^{-1}[u] + \hat{S}h_nG\hat{S}^{-1}[u], \tag{2.26}$$

where $G'(G\hat{S}^{-1}[u])$ is the Fréchet derivative of the operator G. The last equation has a structure $h_{n+1}[u] = \hat{M}h_n[u]$, where $\hat{M}$ is the linear operator. One may expect that the asymptotics of the solution h_n will be defined by the superposition of eigenvectors of the operator $\hat{M}$ with larger moduli of eigenvalues. Fortunately, these eigenvalues as well as the nnecessary infor-

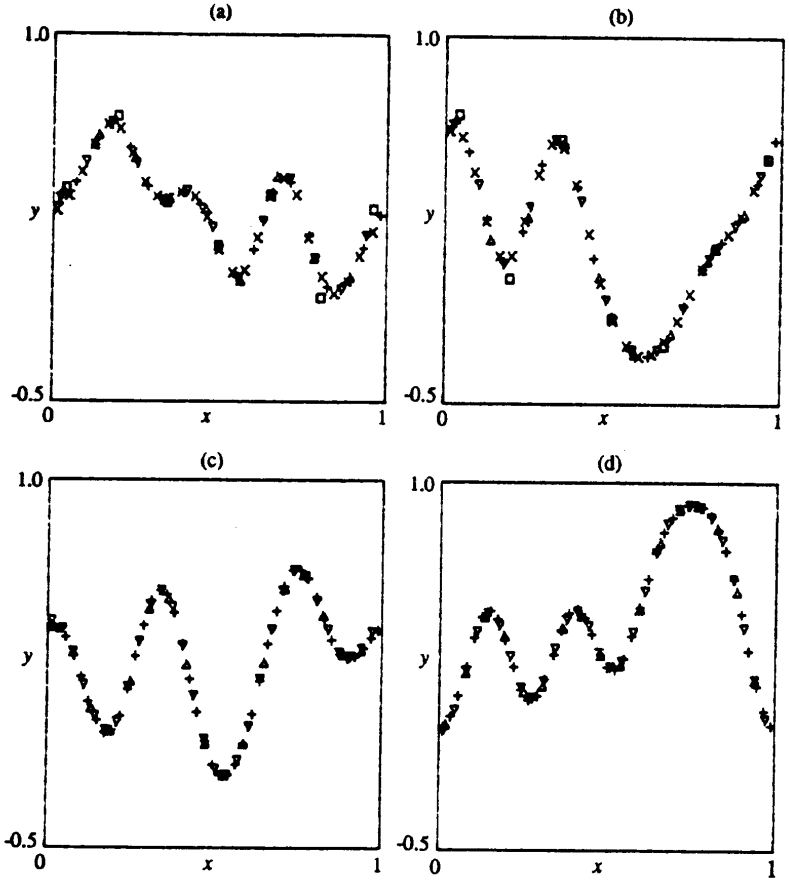

Figure 2.2 Results of numerical verification of existence and universality of the fixed-point operator G for one-dimensional lattices with diffusive coupling for the critical value of the control parameter λ: (a, b) the results of 2(□), 4(△), 8(▽), 16(+) and 32(×) iterations of (2.21) in renormalized form (see text) for two probe initial functions; $D = 0.8$, the number of lattice elements $M = 26, 37, 52, 73, 104$; (c, d) the results of 32 iterations with two probe initial functions for three models : the future coupling system (2.21) with $D = 2(+)$ and systems of form (2.25) with $\hat{L}$ being the averaging operator over 3(△) and 5(▽) neigbours.

mation about the structure of the eigenvectors may be found without formal solution of the operator eigenproblem.

Let us return to the universal representation of the evolution operator near the lattice fixed point and include only the perturbations responsible for the diffusion and one of the additional types of coupling, for example A :

$$u_{l+1,m} = g(u_{l,m}) + A[\phi_1(u_{l,m}, u_{l,m+1}) - \phi_1(u_{l,m}, u_{l,m-1})] + D[\phi_2(u_{l,m}, u_{l,m+1}) + \phi_2(u_{l,m}, u_{l,m-1})], \quad (2.27)$$

Let

$$A \ll D \ll 1, \quad (2.28)$$

i.e. the diffusion dominates. Now we can choose one of two ways.

The first way is to proceed immediately to the continuum limit by replacing differences by spatial derivatives in (2.27) and then performing the RG transformation (2.23) n and $n+1$ times. Thanks to (2.28) it is possible to select n so as to provide operators $G_n = G + Ah_n$ and $G_{n+1} = G + Ah_{n+1}$ close to the fixed point G.

The second way is first to perform the lattice RG transformation (Section 2.2.2), proceed to the continuum limit, and then rescale the spatial variable by $\sqrt{2}$. Then, the diffusive term does not change while the A-type term accepts the factor $a/\sqrt{2}$. Then we perform the RG transformation (2.23) n times and obtain the operator $\tilde{G}_n = G + Ah_n a/\sqrt{2}$, which must coincide with the above operator G_{n+1}. So, we have $h_{n+1} = h_n a/\sqrt{2}$, i.e. the operator that arises from the given initial perturbation through n steps of renormalization is just the eigenvector of equation (2.26) with eigenvalue $v_1 = a/\sqrt{2} = -1.7698$. We denote this eigenvector by H_1. In a similar manner, we can show that including other additional types of coupling gives the eigenvectors H_2 and H_3 with eigenvalues $v_2 = \sqrt{2} = 1.4142$ and $v_3 = a/2 = -1.2512$. Of course, the eigenvector H_0 must be added with eigenvalue $\delta = 4.6692$ corresponding to perturbation of the local map control parameter.

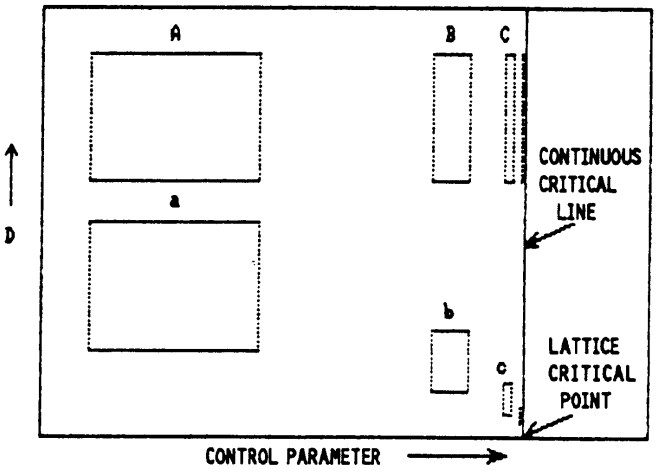

Figure 2.3 Explanation of relation between lattice and continuous scaling for the system with diffusion. The sequences of the regions are shown in the same sense for the former (a, b, c) and latter (A, B, C) types of scaling.

Thus, we can now give the formulation of the *continuous scaling*.

In the continuum limit the spatially distributed system with dominating diffusion is characterized by four essential parameters $\Lambda, \alpha, \beta, \gamma$—the coefficients at the eigenvectors H_0, H_1, H_2, H_3. The space of the parameters has the property of scale invariance under change of parameters $\Lambda \to \Lambda/\delta$, $\alpha \to \alpha/v_1$, $\beta \to \beta/v_2$, $\gamma \to \gamma/v_3$ accompanied by rescaling of the dynamical variable u by $1/\alpha$, doubling of the temporal scale, and increasing of the spatial scale by $\sqrt{2}$.

Figure 2.3 explains the relation between lattice scaling and continuous scaling for the simplest case of the system with pure diffusion. In the plot of the control parameter against the coupling constant the critical point associated with the fixed point of the lattice RG transformation exists, and the critical line occurs where the long time evolution operator converges to the universal operator G. Two sets of regions are also shown, which are similar in the sense of the lattice scaling (a, b, c) and in the sense of the continuous scaling (A, B, C).

2.3 Lattice scaling in the dynamics of coupled map systems

The aim of our further study is to show what conclusions may be drawn about the spatiotemporal dynamics of the CMLs on the basis of a developed RG approach. In this section we restrict ourselves to systems with symmetric coupling and concentrate our attention on lattice scaling. The concept of scaling will lead us to the organizing principle of the hierarchical structure of parameter space near the critical situation. But to reveal this structure we must turn to computer simulation. Here we use results obtained by several authors. So, some inconsistency in notation and normalization of dynamical equations is inevitable.

The simplest illustration of lattice scaling is the system of two coupled period-doubling maps. It plays here only a subsidiary role, so the reader is referred to specialized works [30–34] for detailed discussion of its dynamics. We shall only consider some examples of similar sustained dynamical regimes.

In the left-hand columns of Figures 2.4 and 2.5 a general view of attractors is given for the systems of two maps (2.12) and (2.15) for the cases of pure dissipative and pure inertial coupling, respectively. The parameters change downwards in accordance with the appropriate scaling rule $(\lambda - \lambda_0) \to (\lambda - \lambda_0)/\delta$, $\varepsilon \to \varepsilon/2$ or $\varepsilon \to \varepsilon/\alpha$. In the right-hand columns the magnified parts of the pictures are reproduced which correspond to the marked rectangles. Their similarity supports the expected scaling. Rigorously speaking, the scaling is asymptotic and the coincidence is better for higher levels the resolution.

Notice that in order to observe the similarity of dynamics not only is the above parameter rescaling necessary, but also the initial condition for the

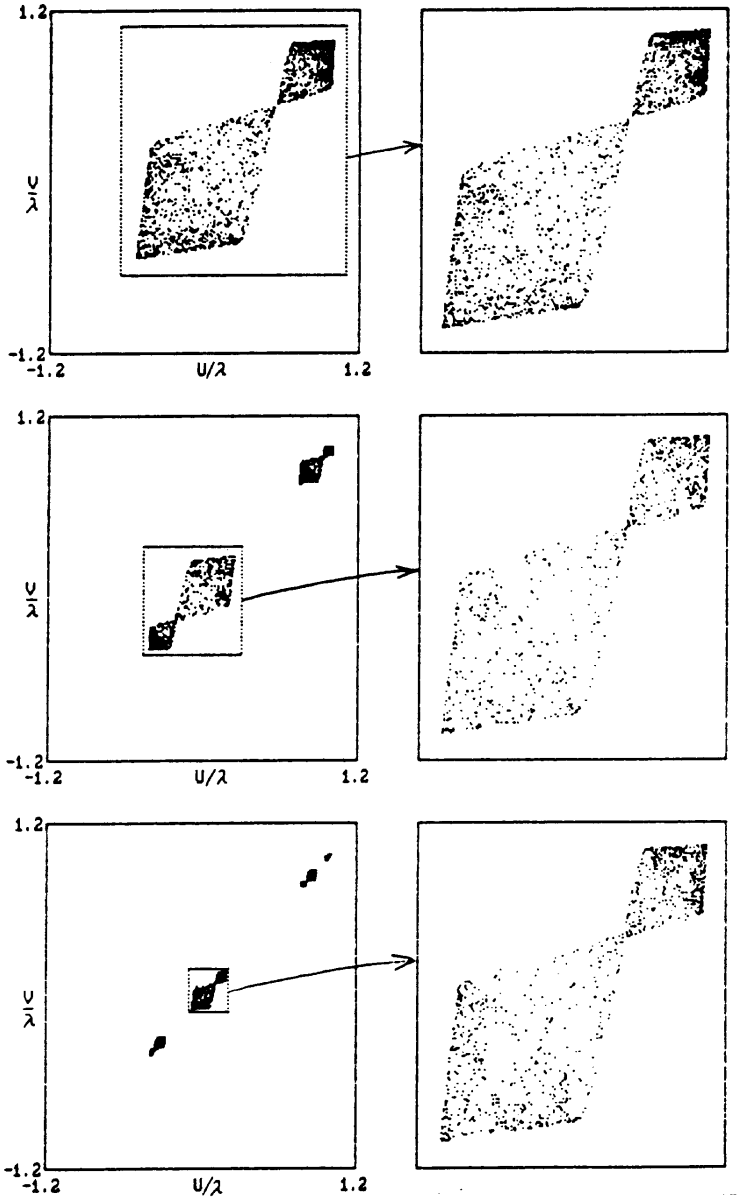

Figure 2.4 Illustration of scaling in dynamics of two dissipatively coupled maps (2.12) with $f(u) = \lambda - u^2$. The left-hand column shows the general view of attractors for $\lambda = 1.54$, $\varepsilon = 0.06$; $\lambda = 1.43089$, $\varepsilon = 0.03$; $\lambda = 1.40752$, $\varepsilon = 0.015$, respectively (ε is halved from one picture to the next the difference $\lambda - \lambda_0$ decreases by δ). The right-hand column depicts the magnified parts inside the smaller rectangles.

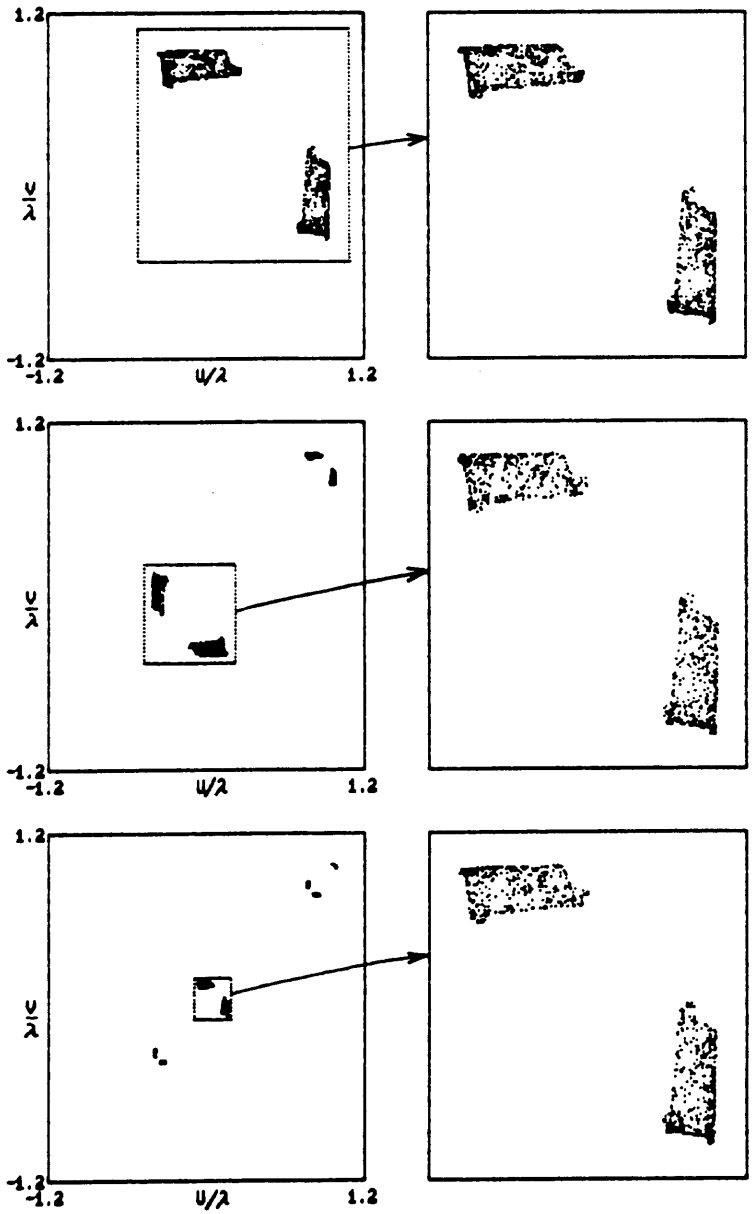

Figure 2.5 Illustration of scaling in dynamics of two systems with inertial coupling (2.15) for $\lambda = 1.54$, $\varepsilon = 0.06$; $\lambda = 1.43089$, $\varepsilon = -0.02397$; $\lambda = 1.40752$, $\varepsilon = 0.009578$, respectively. In contrast to Fig. 2.4 the coupling parameter is rescaled by a.

system must hit into the basin of the desired attractor. This reservation is essential because the coupled maps exhibit multistability only near the considered critical point $(\lambda_0, 0, 0)$. In fact, if the uncoupled maps move with a period of 2^n then they may have an arbitrary phase shift by 0, 1, 2, 3, ..., $2^n - 1$ steps, thus many different states of the composite system appear. Also they are preserved under inclusion of sufficiently weak coupling.

Returning to the spatially extended CML we start again from the lattice with diffusive coupling and take the dynamical equation in the form used by Kaneko [8, 29] :

$$u_{l+1,m} = 1 - \lambda u_{l,m+1}^2 - (\varepsilon\lambda/2)(u_{l,m+1}^2 - 2u_{l,m}^2 + u_{l,m-1}^2). \qquad (2.29)$$

with boundary conditions of periodicity $u_{l,0} = u_{l,M}$. This is just the model (2.20) with $f(u) = 1 - \lambda u^2$ and $D = \varepsilon/2$.

When the control parameter λ exceeds the value $\lambda_1 = 0.75$ (at which the stable period-2 cycle of the local map appears), the expanded systems have the possibility of forming *domains*. Each domain is formed by the lattice cells oscillating with the same phase. The location of the domains and their sizes depend on the initial conditions for the lattice.

For larger λ the variety and complexity of the possible domain structures increase. Let us sketch the principle of their classification. It is known that near the critical point λ_0 the long-period cycles of the local map have a hierarchical organization. Their elements are grouped into a sequence of clusters with decreasing sizes. There are two clusters at the 1st level, four clusters at the 2nd level and so on (see Fig. 2.6). The connected part of the lattice where the instantaneous states of the cells are related to the same cluster at the nth level we call the domain of the nth order. The spatial region that demarcates the domains of the nth order is called the domain wall of the

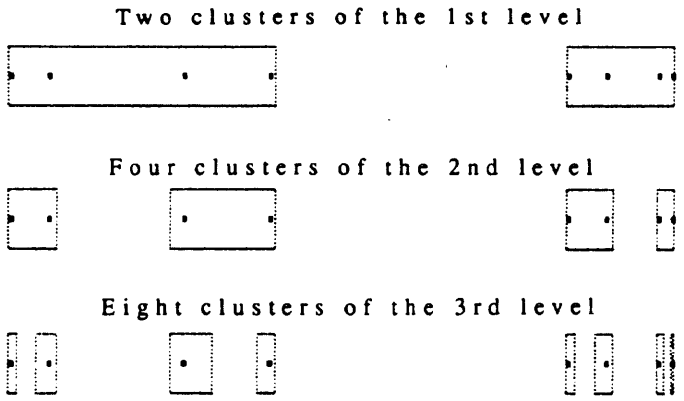

Figure 2.6 Cluster structure of the local map attractor in the subcritical range. An example of a period-8 cycle.

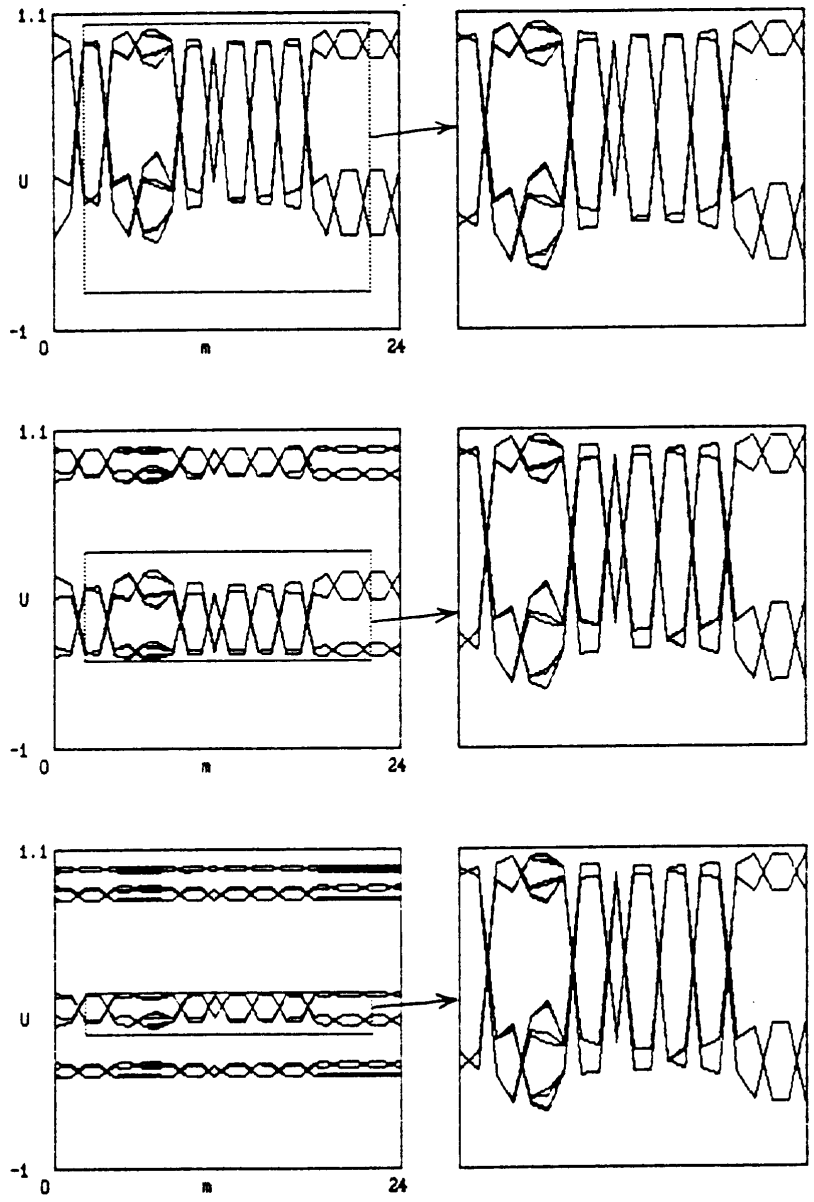

Figure 2.7 Lattice scaling in CML with pure diffusion (2.29). The parameters are $\lambda = 1.44400$, $\varepsilon = 0.1$; $\lambda = 1.41033$, $\varepsilon = 0.05$; $\lambda = 1.40312$, $\varepsilon = 0.025$, respectively. The right-hand pictures show the parts of the left-hand ones inside the smaller rectangles with vertical size decreasing from one picture to the next by a while the horizontal size is unchanged.

nth order. If the length of the domain is sufficiently large other domains of higher orders exist inside it.

Let us assume that a certain domain structure is formed for definite values of λ and α. The property of the lattice scaling allowes us to conclude that a similar spatial structure may be realized for $\lambda \to \lambda_0 + (\lambda + \lambda_0)/\delta$, $\varepsilon \to \varepsilon/2$, $u_m \to u_m/\alpha$ with doubling temporal period. Figure 2.7 shows such an example. The first picture was obtained for $\lambda = 1.444$ and $\varepsilon = 0.1$ with random initial conditions. The spatial configurations for several sequential temporal steps are shown after finishing the transients. Then the rescaling of λ, ε and u was undertaken, and the spatial configurations are again depicted after the decay of transients. Three levels of the rescaling are presented in the left-hand column of Figure 2.7. To make the similarity of the structures evident, the parts of them inside certain rectangles are plotted magnified in the right-hand column. The magnification along the vertical axis is proportional to a^n (n is the level number) according to the expected scaling. The similarity of the pictures may be clearly seen.

In the supercritical region of λ the CML with diffusive coupling exhibits a variety of types of behaviour—phases classified by Kaneko [8, 29]. His phase diagram in the (λ, ε) plane of the model (2.29) is reproduced in Figure 2.8. The regions of different phases are labelled FRP (frozen random pattern), PS (pattern selection), BD (Brownian motion of defects), DT (defect turbulence), PCI (pattern competition intermittency) and FDT (fully developed turbulence). Thanks to the RG analysis, one may suppose that the same pattern of Kaneko phases is reproduced many times in decreasing scales near the lattice critical point (see Fig. 2.8). The transition to the next level of scaling, i.e. the realization of the Kaneko phases inside the smaller

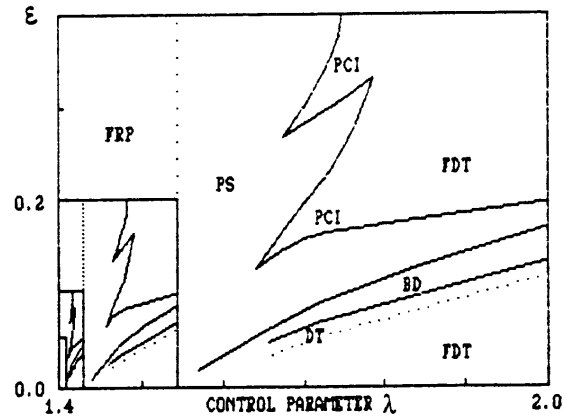

Figure 2.8 Kaneko phase diagram for CML with pure diffusion (2.29) with added fragments reproducing the same phases near the critical point $\lambda = 1.401155$, $\varepsilon = 0$. See the text for explanation of the abbreviations.

rectangle in the figure demands that we decrease the amplitude of random initial conditions by a times. Figure 2.9 shows examples of spatiotemporal diagrams similar to those presented in [8, 29], but relating to the second level of scaling.

Of course, under transition from the first to the second level only approximate reproduction of the forms of the regions occurs because we are attempting to apply the scaling property to too large a domain of the parameter space. Closer and closer reproducibility is expected for higher levels.

Let us now consider the lattice with intertial coupling between the cells.

$$u_{l+1,m} = \lambda - u_{l,m}^2 + C(1 - 0.176u_{l,m})(u_{l,m+1} - 2u_{l,m} + u_{l,m-1}). \quad (2.30)$$

again with periodicity conditions $u_{l,0} = u_{l,M}$. The similar system with linear coupling was considered by Waller and Kapral [9], but for our model the scaling property will be observed with higher precision thanks to its special form.

In the central part of Figure 2.10 the view of the parameter plane (λ, C) is presented showing the domain of stability of spatially uniform states for the asymptotically long system $M \gg 1$. The parts of the boundary denoted by Z correspond to the 'zigzag structure' that appears with a wavelength of 2 (see examples in the upper pictures of Fig. 2.10). The part of the boundary K is associated with structures that arise with larger wavelengths depending on where we cross the boundary (see the examples in the lower pictures of Fig. 2.10). The horizontal lines are the lines of temporal period-doubling for the spatially uniform state. The asymptotic scale invariance was previously noted in [9] and there it was explained for the configuration of the stability domain reproduced under parameter change by the factors of δ and α along the coordinate axes. According to our RG analysis, the scaling properties are inherent not only in almost uniform states, connected with self-similarity of the stability region, but also hold for a variety of complex spatial structures which may arise in the lattice. The upper and lower pictures in Figure 2.10 correspond to the points of similarity in the parameter plane. The initial conditions used coincide us to a characteristic scale of u (differ by a). One can see that the configurations inside the small rectangles are similar.

2.4 Continous scaling and dynamics of coupled map lattices

Proceeding to the continuum limit in lattices with diffusion may be done in two cases: (1) when the coupling is initially large and immediately makes the states of the neighbouring cells close (this is just the case of the future coupling models with $D \gg 1$), and (2) when those states near the critical situation with $\lambda - \lambda_0 \sim \delta^{-n}$ are considered which have the characteristic scale of the dynamical variable $\Delta u \sim a^{-n}$ for some fixed D. So, the dynamics are governed by the n-fold renormalized evolution operator with the characteris-

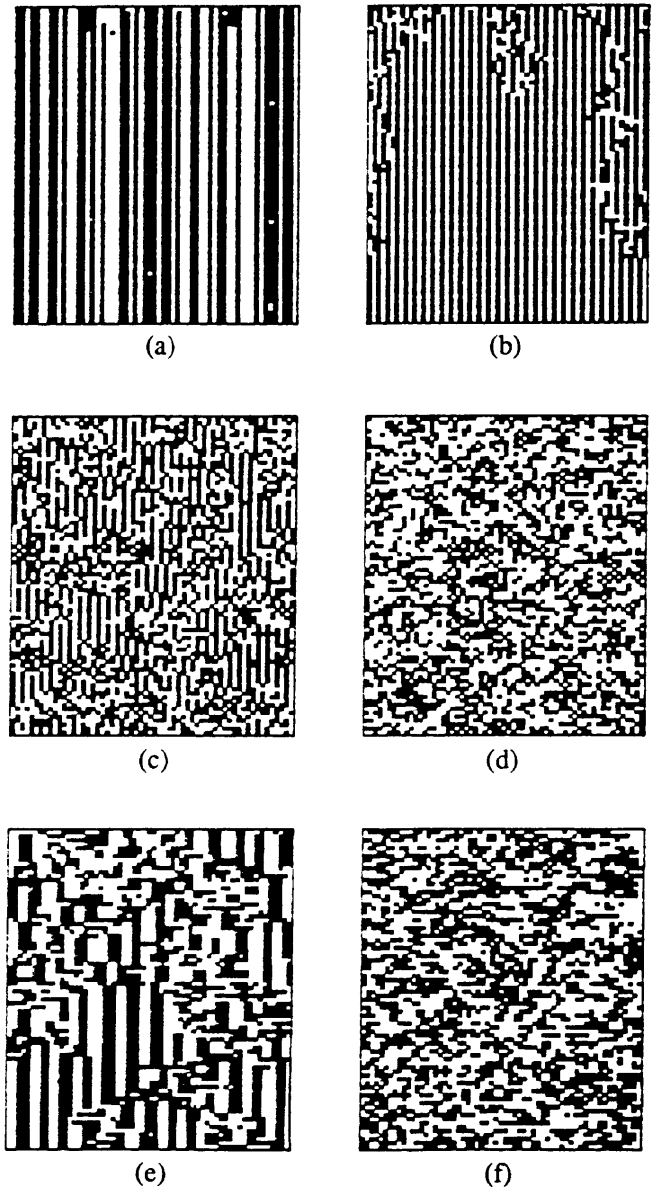

Figure 2.9 Space-time diagrams reproducing Kaneko phases inside the smaller rectangle in Fig. 2.8 : (a) PS, $\lambda = 1.444$, $\varepsilon = 0.05$; (b) BD, $\lambda = 1.483$, $\varepsilon = 0.05$; (c) DT, $\lambda = 1.492$, $\varepsilon = 0.05$; (d) FDT, $\lambda = 1.54$, $\varepsilon = 0.05$, (e) PCI, $\lambda = 1.474$, $\varepsilon = 0.15$; (f) FDT, $\lambda = 1.528$, $\varepsilon = 0.15$. The spatial index is plotted along the horizontal axis and the time index downwards along the vertical axis. The number of lattice cells is 60; each 64th time step is shown. The pixesl are white or black according as u is greater or less than the smallest element of period–2 cycle of the local map.

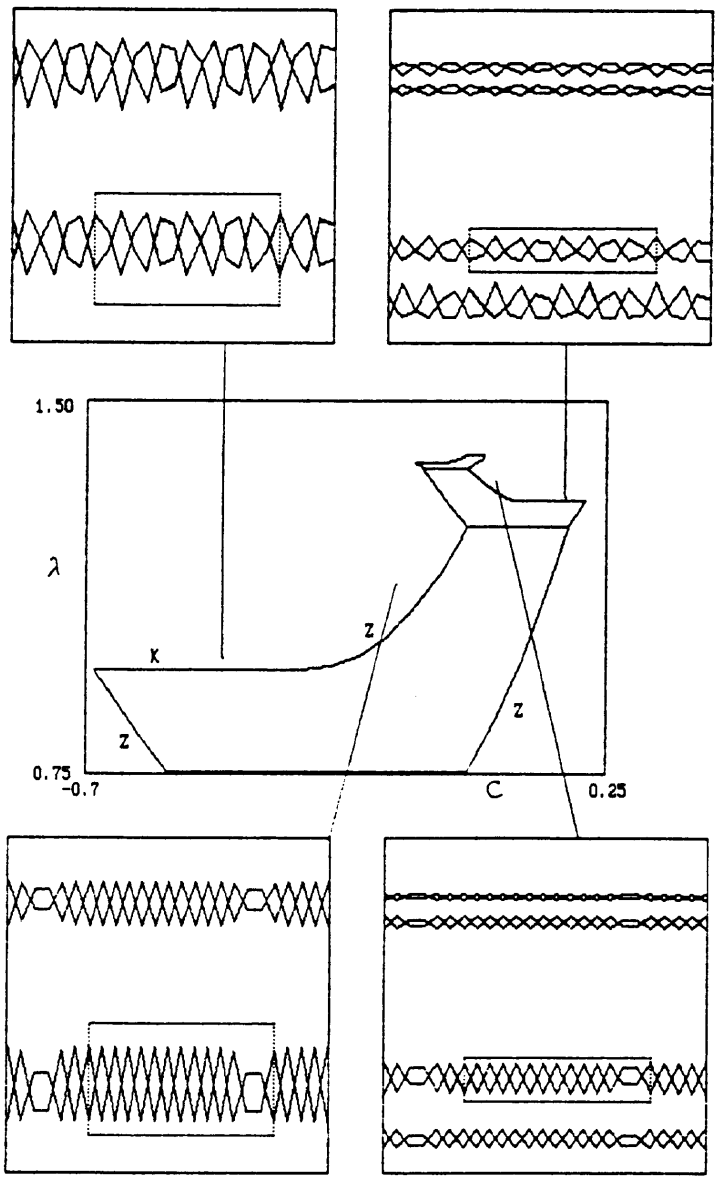

Figure 2.10 Domains of stability for spatially uniform states of the long lattice with inertial coupling and examples of sustained dynamical regimes in several points of the parameter plane. The configurations inside the rectangles in the top pictures have the same relationship as those in the lower pictures.

tic spatial scale (diffusion length) $\sim \sqrt{D}\cdot 2^{n/2}$ greater than the lattice step. This is also valid when the additional types of coupling are presented with sufficiently small coefficients. These situations are attractive for theoretical investigation because of the decreasing number of essential parameters. In particular, only one of them (λ) remains in the case of an asymptotically long system with pure diffusion. In this section we start from this case and then consider the inclusion of small additional transfer and inertial coupling.

2.4.1 *Domain structures in coupled map lattice with pure diffusion*

We have already considered the increasing variety of domain structures appearing when the control parameter λ goes to the critical value. For the systems diffusion coupling the width of the domain walls and the smallest allowed size of the domains increases with the order n proportionally to $2^{n/2}$ due to the continuous scaling. At the points of similarity in the λ-axis (where the ratio of values $\lambda - \lambda_0$ is δ) the domain walls of the nth and $(n+1)$th order must have similar form and the ratio of spatial scales is $\sqrt{2}$. This property is illustrated in Figure 2.11. In the left-hand column are shown the spatial configurations containing the domain walls of the order $n = 1, 2, 3$ for the future coupling model (2.21). Also depicted are the rectangles whose size decreases as a^{-n} in the vertical direction and increases as $2^{n/2}$ along the horizontal axis by the rule of continuous scaling. In the right-hand column the parts of the pictures fitting into the rectangles are reproduced. Comparison of these allows us to see that the scaling property works well, except at the lowest level.

The next interesting property of the domain structures, which has been noted by several authors in their computations, is the almost complete independence of the dynamics inside the domain from that of neighbouring domains [7, 10, 11, 22]. In orther words, the structures with large temporal periods do not penetrate deeply into the domain walls of the lower order. For this reason, the domain may be considered as a solitary quasi-isolated system. Its dynamics are governed by only two essential parameters—λ and the domain length M.

In the pure form one can study the dynamics of the one-domain states by taking the system of finite length under fixed end boundary conditions. It is remarkable that their concrete form is inessential.

To understand the last statement let us start from the case of the semi-infinite future coupling system with only one fixed end ($u_{l,0} = 0$) and consider the structure that arises from the uniform initial condition $u_{0,m} = 0$ at the critical point $\lambda = \lambda_0$. The result of the computation after ignoring transients is shown in Figure 2.12. (The full length of the system $M = 1000$ is much greater than that part shown.) This is *the universal scale-invariant pattern*. Its configuration is shown after rescaling along the axes by a and $\sqrt{2}$ (see the lower pictures). Notice that the scaling centre of the pattern does not

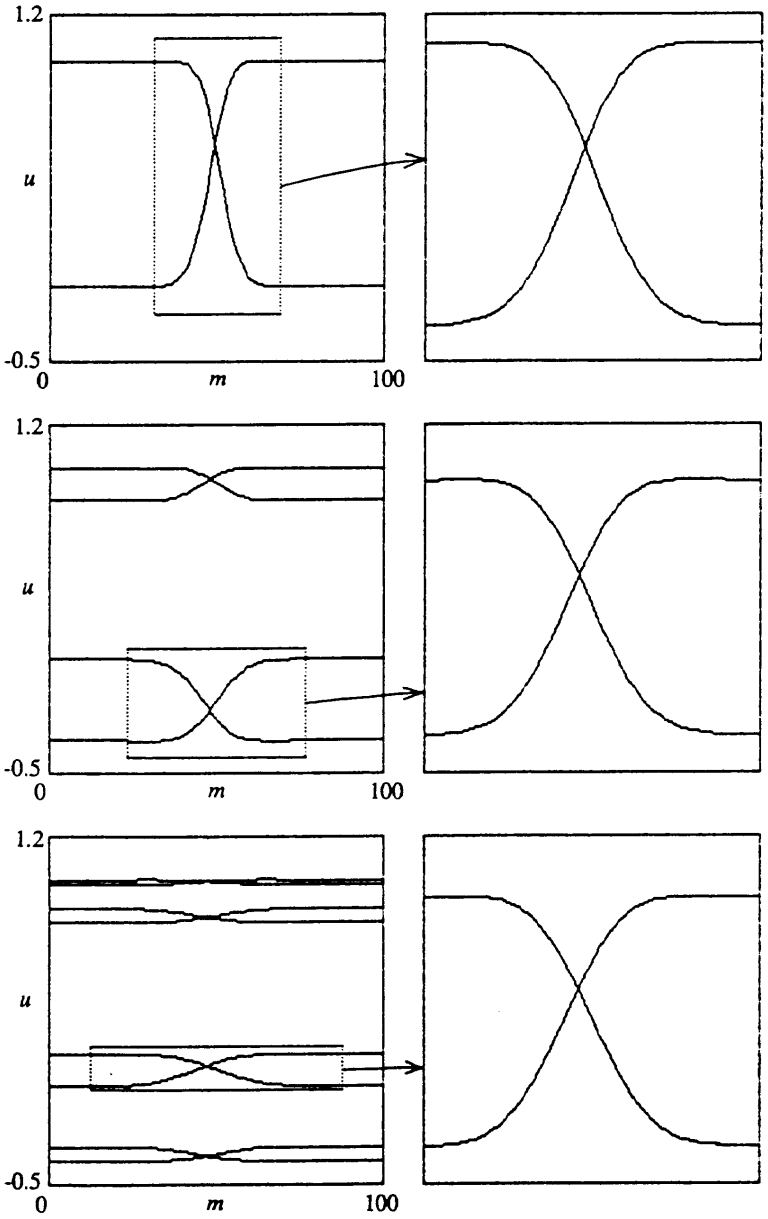

Figure 2.11 Continuous scaling of the domain walls of different levels for the future coupling system (2.21), $D = 8$, $M = 100$ with periodic boundary conditions. The left-hand pictures show the general view of space–amplitude plots for $\lambda = 1.2$, 1.35807, 1.39193. Those on the right depict the parts of the structures inside the rectangles whose vertical sizes decrease from level to level by a while the horizontal sizes increase by $\sqrt{2}$.

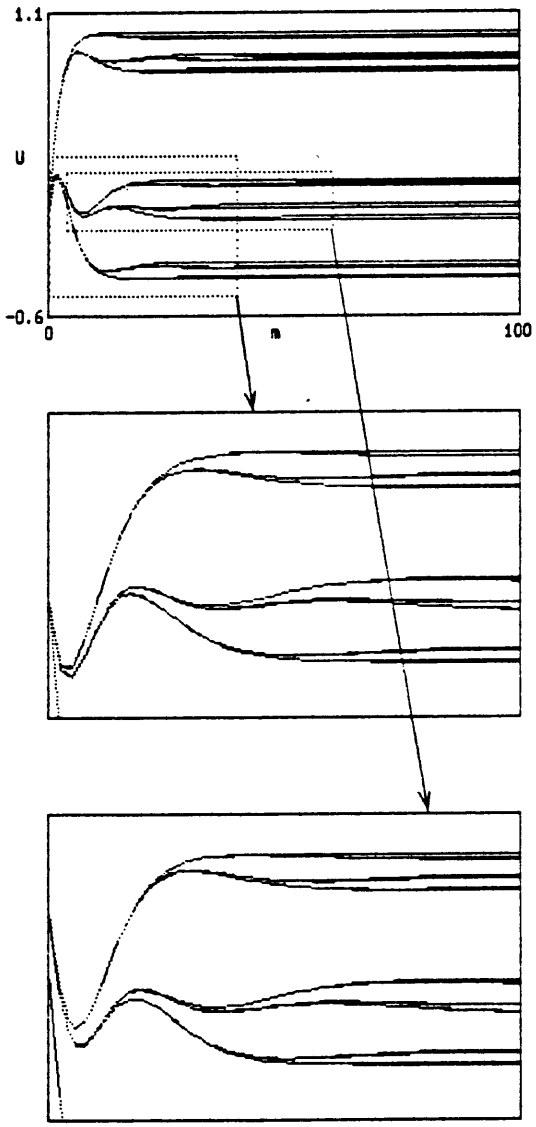

Figure 2.12 Space–amplitude plot for universal pattern near local dislocation in the critical situation $\lambda = \lambda_0$. The 2nd and 3rd pictures reproduce those parts of the pattern inside the rectangles marked in the 1st picture.

coincide with the end of the lattice, but lies at some distance Δ outside the system. For the case under consideration $\Delta \simeq 4.5\sqrt{D}$. At some distance from the end the pattern would have the same form for any fixed-end boundary conditions $u_{l,0} = C < 1$. Only the value of Δ depends on the constant C.

Returning to the system with finite length $M \gg 1$ we will have two ends with the formation of the above universal patterns near each of them. In the subcritical region they will interact by their tails. This leads, in particular, to some shift of period-doubling bifurcations. Because of the continuous scaling we may assume they satisfy the relation

$$\lambda_n = \lambda_0^0 - K^0 \delta^{-n} \varphi(\theta \cdot 2^{-n/2}), \tag{2.31}$$

where φ is the universal function, $\theta = (M + 2\Delta)/\sqrt{D}$, λ_n^0 and K^0 are constants in Feigenbaum's relation for the local map ($\lambda_n^0 = \lambda_0^0 - K^0\delta^{-n}$, and in particular for $f(u) = 1 - \lambda u^2$ we have $\lambda_0^0 = 1.401155$ and $K^0 = 0.7245$). Equation (2.31) was varified by special data-processing procedure with very high precision [10, 21].

A general view of the parameter plane (λ, M) and some examples of ensuing spatial configurations are shown in Figure 2.13. Consider the evolution of the one-domain state under the adiabatically slow increase of λ. Initially the period-doubling bifurcations are observed at approximately the same values of λ_n^0 as for the local map (hence we find $\varphi(\xi) \to 1$ for $\xi \to \infty$). However, the above-discussed universal patterns begin to form near the ends, initially at the lowest levels of its structure. The spatial scale of the tails increases with the bifurcation number as $2^{n/2}$. Beginning with some n the length of the tails becomes comparable with the system size, so the bifurcation points essentially perturb. The computations show that the period-doubling bifurcations continue. Here the characteristic spatial scale of the evolution operator through the period of the cycle would be greater than the system length. Thus, the system again becomes equivalent to a one-dimensional map with Feigenbaum's law of the accumulation of subsequent period doublings $\lambda_n = \lambda_0 - K\delta^{-n}$ but with new λ_0 and K. It may come to agree with the relation (2.31) by an assumption that for $\xi \to 0$ the function $\varphi(\xi)$ behaves as

$$\varphi(\xi) = -(\xi/A)^{-\chi} + B, \tag{2.32}$$

where A, B and $\chi^4 2 \log_2 \delta = 4.4463$ are universal because of the universality of $\varphi(\xi)$. Substituting (2.32) into (2.31) we obtain the relations

$$\lambda_0 = \lambda_0^0 + K^0(\theta/A)^{-\chi}, \quad K = BK^0. \tag{2.33}$$

Numerical estimation based on the data of Figure 2.13 gives $A \approx 12.8$, $B \approx 1.08$.

Behaviour equivalent to that of a one-dimensional map also applies for supercritical λ so long as the difference $\lambda - \lambda_0$ is sufficiently small. Here temporal chaos with simple one-hump spatial structure and windows of regularity for some narrow intervals of λ are realized. By increasing λ and/or θ we may achieve chaotic modes with more complicated spatial structures or observe jumps to regular states containing the domains of higher order.

Using the above information on the dynamics of a single domain, we may

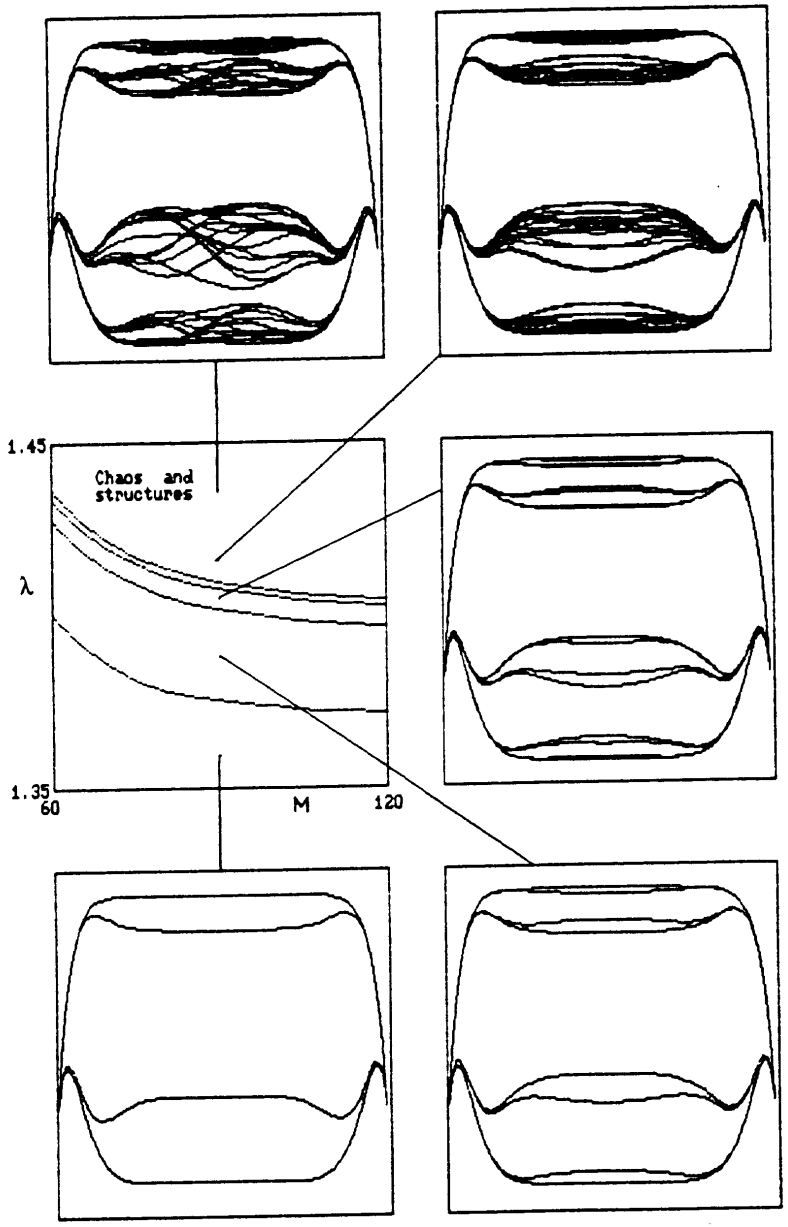

Figure 2.13 Parameter plane (length M vs. control parameter λ) for one-domain state of future coupling system (2.21) with fixed-end boundary conditions ($u_{l,0} = 0$, $u_{l,M} = 0$) and some examples of space–amplitude diagrams for points of the plane after decay of transients. The initial conditions $u_{0,m} = 0$ are used.

come to some conclusions about the behaviour of the multi-domain states in a long system. Let us suppose that such a state is formed for a subcritical value of the control parameter. Then increasing λ leads to transition to chaos initially inside the larger-length domains while the regular temporal behaviour is preserved for the shorter ones. Keeler and Farmer [11] have shown that in this case random movement of the domain walls is observed. So, the chaotic dynamics in some domain may change to the regular one and vice versa, giving rise to the specific spatiotemporal intermittency discovered in [11].

Continuous scaling may also be illustrated for the developed chaotic states where the domains structure is completely destroyed. We notice the remarkable circumstance that such states may be realized for an arbitrary small supercriticality $\lambda - \lambda_0$. As an illustration consider the lattice with future coupling and periodic boundary conditions. The value of λ correspond to the points of band-merging for the local map and the initial conditions are given as almost uniform spatial states with small random perturbations. Each picture on the left-hand side of Figure 2.14 shows several consecutive spatial configurations after some large number of preliminary iterations. The spatiotemporal chaos that develops is observed in all cases. However, the 2^n-band structure of the local map attractor is preserved. The parts of the pictures inside the smaller rectangles (with vertical size decreasing as a^{-n} and horizontal size increasing as $2^{n/2}$) are reproduced on the right-hand side of the figure. Their comparison appears to qualitatively support the expected scaling in a statistical sense. Quantitative verification of it in terms of the spatial correlation function was discussed in [22].

2.4.2 *Scaling properties of systems with diffusion and weak additional types of coupling*

From the RG point of view, in this section we deal with the vicinity of the fixed point G. It was shown (Section 2.2.4) that there are three essential types of perturbations responsible for coupling and each has its own scaling factor associated with it. They correspond to inclusion of antisymmetric inertial coupling, antisymmetric dissipative coupling (or transfer), and symmetric inertial coupling. Following [23], we restrict our consideration to those cases with the presence of only one of the additional coupling types in addition to the dominating diffusion and we assume that the length of the system is sufficient to exclude in practice the influence of its finiteness on the character of the dynamics. Then, the number of essential parameters will be 2 (the control parameter λ and one of the coupling coefficients α, β, γ). The lattice models are constructed specially for each case taking into account the results of the RG analysis.

For the system with diffusion and *antisymmetric inertial coupling* let us take the dynamical equation in the form

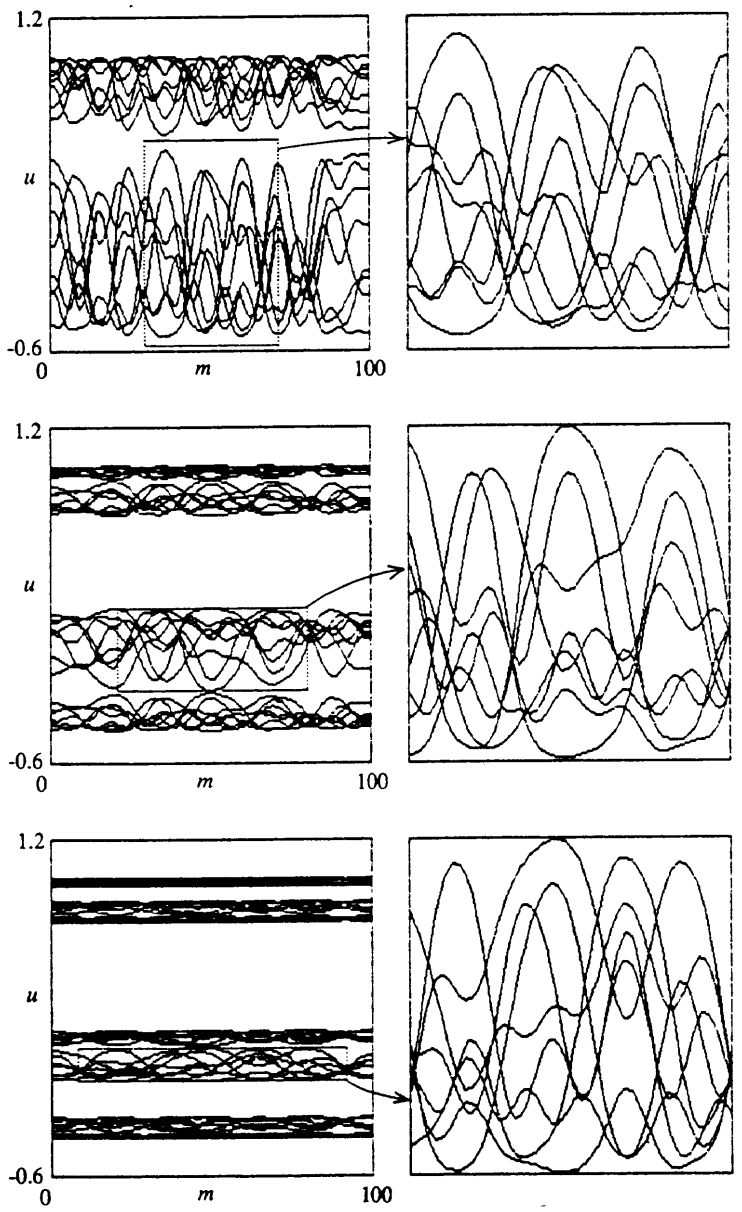

Figure 2.14 Qualitative illustration of scaling in the fully developed turbulent regimes at the points of the local map band-merging.

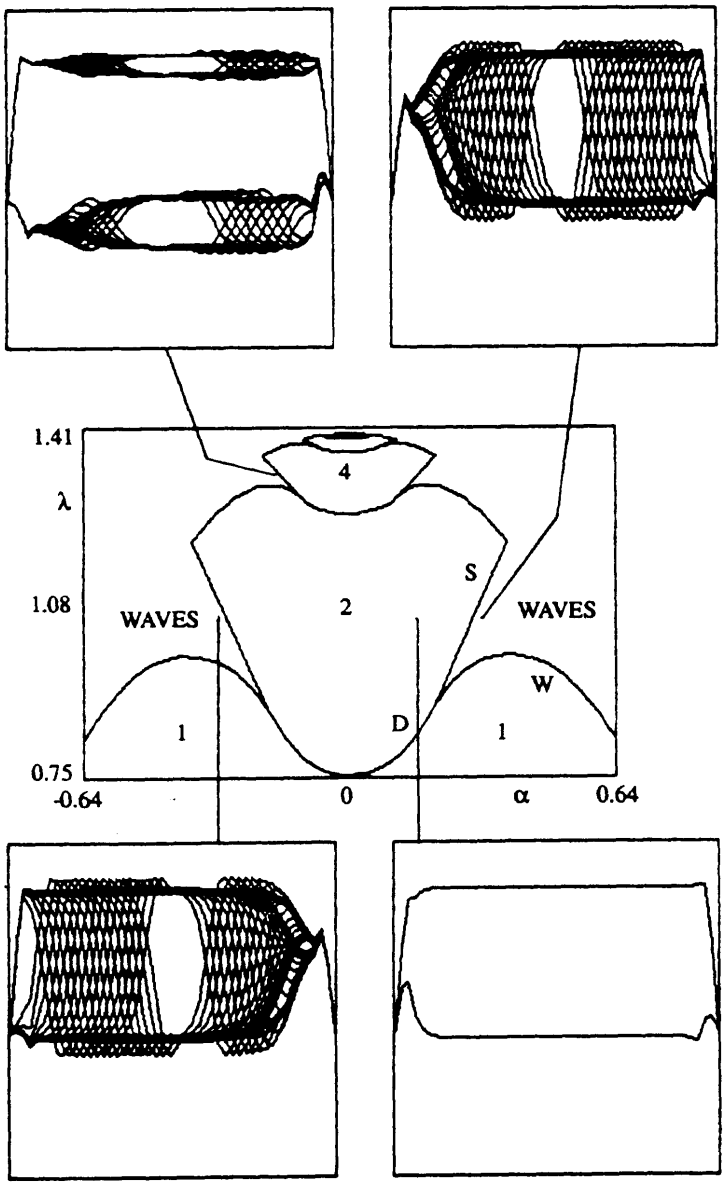

Figure 2.15 The central picture is a parameter plane λ vs. a for the lattice model with diffusion and antisymmetric inertial coupling (2.34). D denotes the line of temporal period doubling of quasi-uniform state, W and S are the lines of the travelling waves that form. The space–amplitude diagrams are shown illustrating the dynamics at several different points of the parameter plane.

$$u_{l+1,m} = \hat{L}[\lambda - u_{l,m}^2 - \alpha(1 - 0,176u_{l,m})(u_{l,m+1} - u_{l,m-1})], \qquad (2.34)$$

where $\hat{L}$ is the averaging operator over three neighbouring sites. The boundary conditions will be the fixed ends: $u_{l,0} = 0$, $u_{l,M} = 0$.

In the central part of Figure 2.15 the parameter plane (λ, α) is shown. There the region of stability may be seen for the quasi-uniform states (i.e. uniform far from the ends) with different time periods. The boundaries of three types are presented [23]. They are the lines of onset of absolute instability via temporal period-doubling (D) and via the travelling waves (W) that appears, and the line of transition from the quasi-uniform to the wave regime because of the formation of the internal source of the waves near one of the system ends (S).

In the upper and lower pictures the characteristic examples of arising spatial configurations are presented for different regions in the parameter plane. The bottom right-hand picture exhibits the quasi-uniform state with temporal period of 2. The bottom left-hand picture shows the quasi-periodic travelling-wave regime, where the domain walls of the 1st order are spontaneously generated and then move from the right to the left. This dynamics occurs against a background of the period-2 state. The top right-hand picture is similar and differs by the sign of the coupling parameter. Here the direction of the movement becomes left to right.

We can see from Figure 2.15 that the plane (λ, α) has a scale-invariant structrure in accordance with the results of RG analysis. The top left-hand picture corresponds to the point in the (λ, α) plane obtained from the previous one by the scaling rule $\lambda \to \lambda_0 + (\lambda - \lambda_0)/\delta$, $\alpha \to \alpha/(\alpha/\sqrt{2})$. We see here the generation and movement of the domain walls of the 2nd order against a background of the period-4 state. The change of the direction of movement in comparison with the initial case is explained by the negativity of the scaling constant $a/\sqrt{2}$.

Figure 2.16 shows the spatiotemporal diagrams illustrating the scaling property for fair sequential levels. The pixel is depicted as black or white according as the sign of the dynamical variable u at the corresponding point is plus or minus. The transition from one picture to the next is accompanied by increasing system length by approximately $\sqrt{2}$ with proportionally decreasing pixel size. Simultaneously, the step between the depicted temporal layers is doubled. The pictures obtained are quite similar (except the lowest level). The alternation of positive and negative pictures is explained by the negativity of the scaling factor a for the dynamical variable.

To obtain the system with diffusion and *transfer* we may use the (2.25) but the linear operator $\hat{L}$ must be modified to $\hat{L}\hat{\Delta}_\beta$, where $\hat{\Delta}_\beta$ is the operator of spatial shift: $\hat{\Delta}_\beta u(x) = u(x - \beta)$ and β is the transfer parameter. The spectrum of the operator $\hat{L}\hat{\Delta}_\beta$ will be

$$e^{-ikx}\hat{L}\hat{\Delta}_\beta e^{ikx} = 1 + i\beta k - (d^2 + \beta^2)k^2/2 + O(k^2).$$

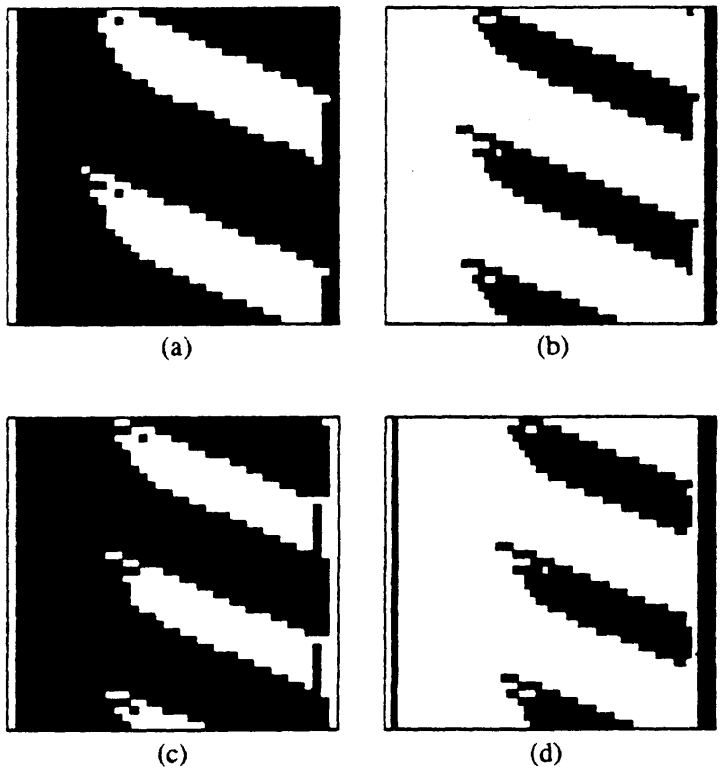

Figure 2.16 Space–time diagrams illustrating scaling of patterns arising in the lattice model (2.34). Boundary conditions of fixed ends $u = 0$ are used. For (a) the 1st picture $\lambda = 1.05$, $a = 0.32$ and each 4th temporal step is shown. For each succeeding picture the temporal interval is doubled, the lattice length is increased by approximately $\sqrt{2}$, the difference $\lambda - \lambda_0$ decreases by δ and the coupling parameter a changes to $a/(a/\sqrt{2})$. The pixel is depicted black if u is positive.

Now we construct the lattice linear operator $\hat{L}_\beta$ with spectrum given by the said relation with $d^2 = 1/2$:

$$\hat{L}_\beta u_m = u_m + \beta(u_{m+1} - u_{m-1})/2 + (1\sqrt{4} + \beta^2\sqrt{2})(u_{m+1} - 2u_m + u_{m-1}). \tag{2.35}$$

and consider the evolution equation

$$u_{l+1,\,m} = \hat{L}_\beta(\lambda - u_{l,\,m}^2). \tag{2.36}$$

The boundary condition will be $u_{l,0} = u_*$, $u_{l,M} = u_*$, where u_* is the fixed point of the local map for the given λ.

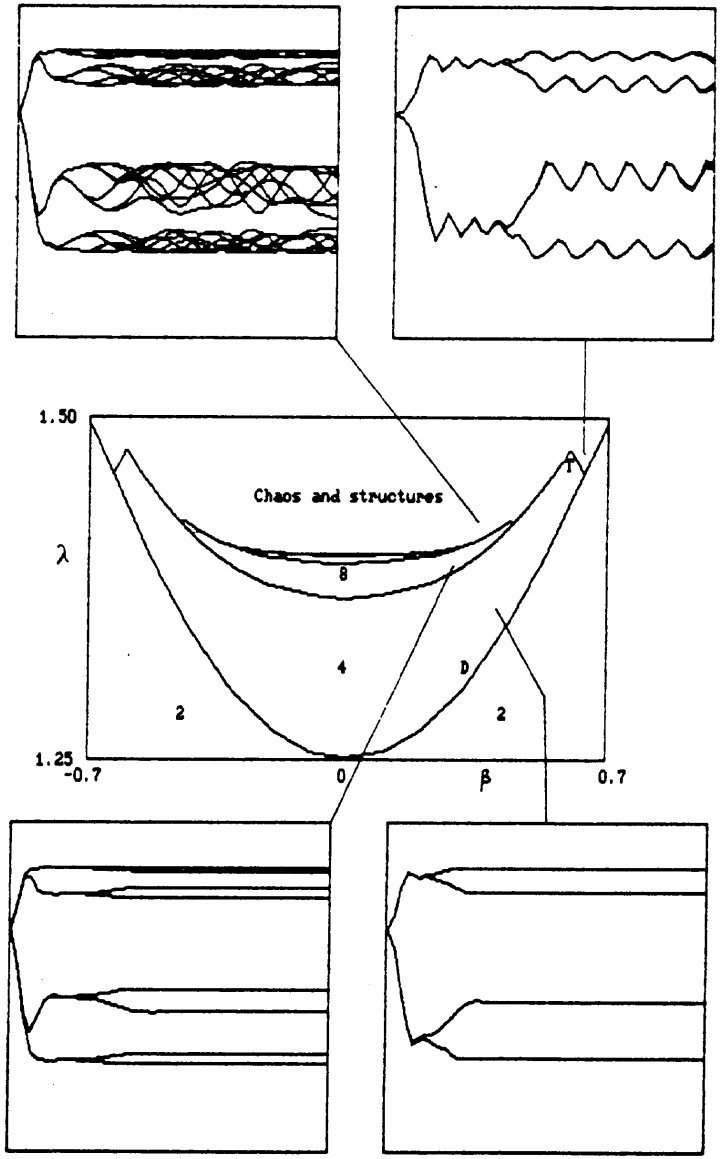

Figure 2.17 The central picture is a parameter plane $\lambda =$ vs. β for the lattice model with diffusion and transfer (2.36). D denotes the line of temporal period-doubling for quasi-uniform state, T is the line of non-dumping spatial oscillations that arise. The space–amplitude diagrams are shown illustrating the dynamics at several different points of the parameter plane.

Figure 2.17 shows the parameter plane (λ, β) and some typical space–amplitude diagrams at representative points of it. The regions of stability for period-2^n quasi-uniform states are bounded by lines of two types. At the lines D the absolute instability of the previous state appears, leading to the temporal period-doubling. At the lines T another route to destruction of uniformity is realized when the oscillating tail penetrating from one of the ends into the system becomes spatially non-dumping (see the top right-hand picture). One of the characteristic peculiarities of the system is the depiction of so-called *spatial period-doublings*. Depending on the parameters, the spatial development leads either to some uniform state with time period 2^n or to the formation of chaotic states through the finite number of spatial period-doublings. The last phenomena were described in [6, 26] for lattices with unidirectional coupling.

Note that the configuration of regions in the (λ, β) plane has a scale-invariant structure. The points of similarity are connected by the scaling relation $\lambda \to \lambda_0 + (\lambda - \lambda_0)/\delta$, $\beta \to \beta/\sqrt{2}$. Figure 2.18 demonstrates the scaling property of spatial patterns arising at such points. The left hand pictures depict the general view of space–amplitude diagrams and the right-hand ones reproduce the parts of them fitting inside the rectangles shown. The similarity of the right-hand pictures is evident.

Turning to the last case of the system with diffusion and *symmetric inertial coupling*, consider the lattice model

$$u_{l+1,m} = \hat{L}[\lambda - u_{l,m}^2 + \gamma(1 - 0.176u_{l,m})(u_{l,m+1} - 2u_{l,m} + u_{l,m-1})], \qquad (2.37)$$

where $\hat{L}$ is defined as the square of averaging operator:

$$\hat{L}u = (u_{m+2} + 2u_{m-1} + 3u_m + 2u_{m+1} + u_{m+2})/9.$$

(This is so the lattice effects decrease in the parameter region that is interesting from the point of view of the presence of bifurcations.) Periodic boundary conditions will again be used.

In Figure 2.19 the parameter plane (λ, γ) is depicted along with space–amplitude plots for some points. The region of stability of uniform states with different time periods may be seen in the centre of the shown part of the (λ, γ) plane. The horizontal bifurcation lines demarcate the regions of period-2^n and period-2^{n+1} spatially uniform regimes. The side boundaries correspond to the appearance of instability at some wavenumber leading to the formation of spatial patterns. This may be considered as spontaneous formation of non-moving domain structure.

According to RG analysis, the form of regions in the (λ, γ) plane must be invariant under the change $\lambda \to \lambda_0 + (\lambda - \lambda_0)/\delta$, $\gamma \to \gamma/(a/2)$. We can see that the reproduction of the picture in smaller scales is governed by this rule. Figure 2.20 gives the evidence of scaling properties for patterns which may be formed at the points of similarity. As before, the left-hand pictures show the

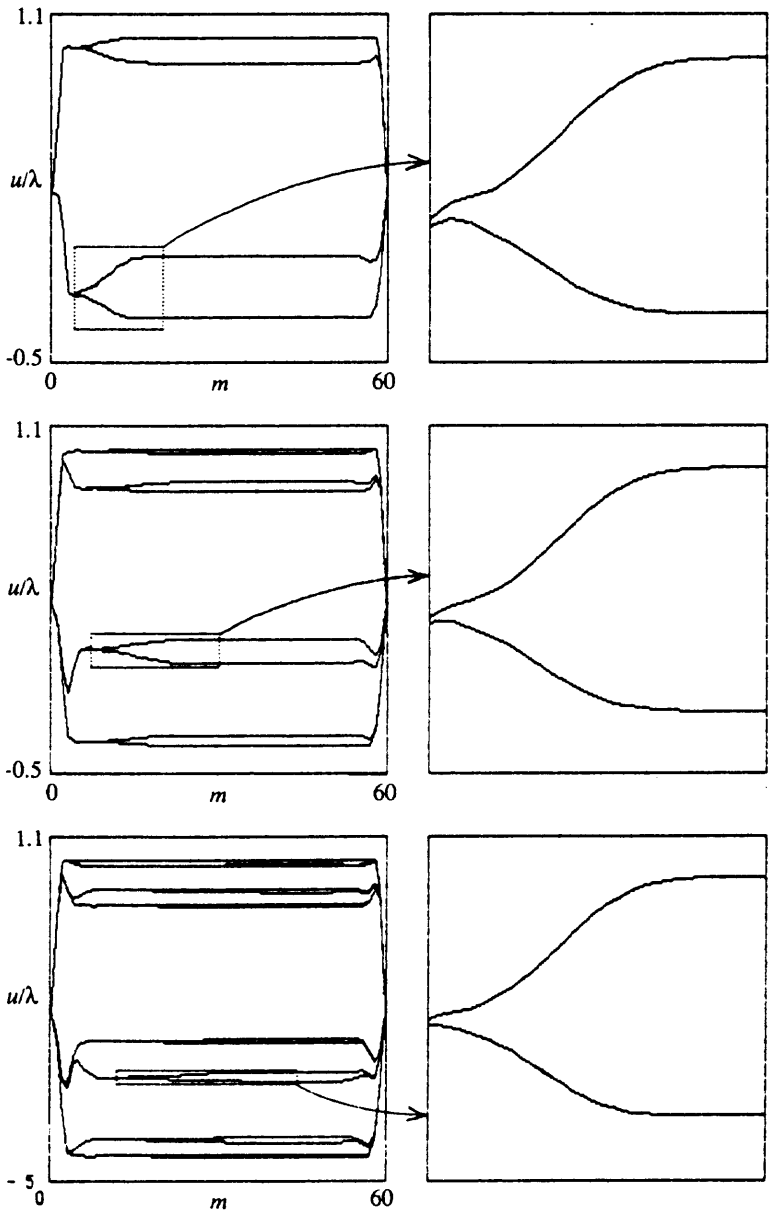

Figure 2.18 Space–amplitude diagrams illustrating scaling in the lattice model (2.36). The fixed-end boundary conditions are taken with the end value of u defined by the fixed point of the local map. The initial conditions are $u_{0,m} = 0$. The values of parameters are $\lambda = 1.3$, $\beta = 0.55$; $\lambda = 1.37949$, $\beta = 0.3889$; $\lambda = 1.39652$, $\beta = 0.275$. The right-hand pictures show the parts inside the marked rectangles.

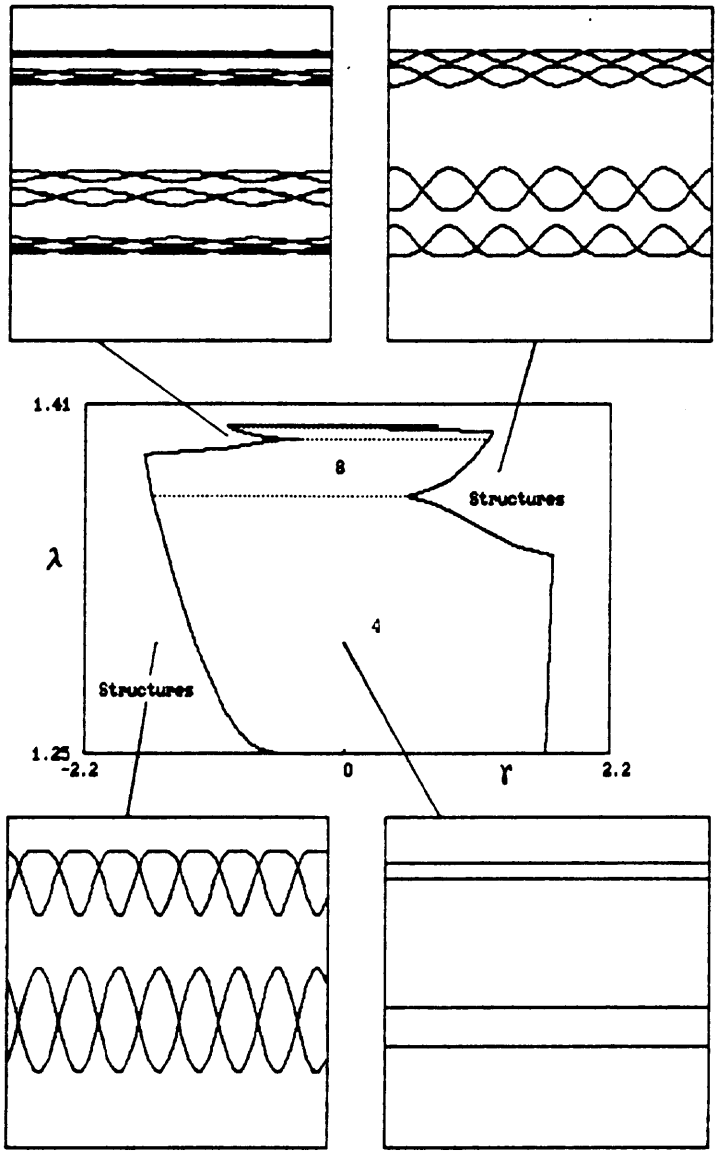

Figure 2.19 Parameter plane λ vs. γ for the lattice model (2.36) with diffusion and symmetric inertial coupling, and space–amplitude diagrams illustrating the dynamics at several different points of the plane.

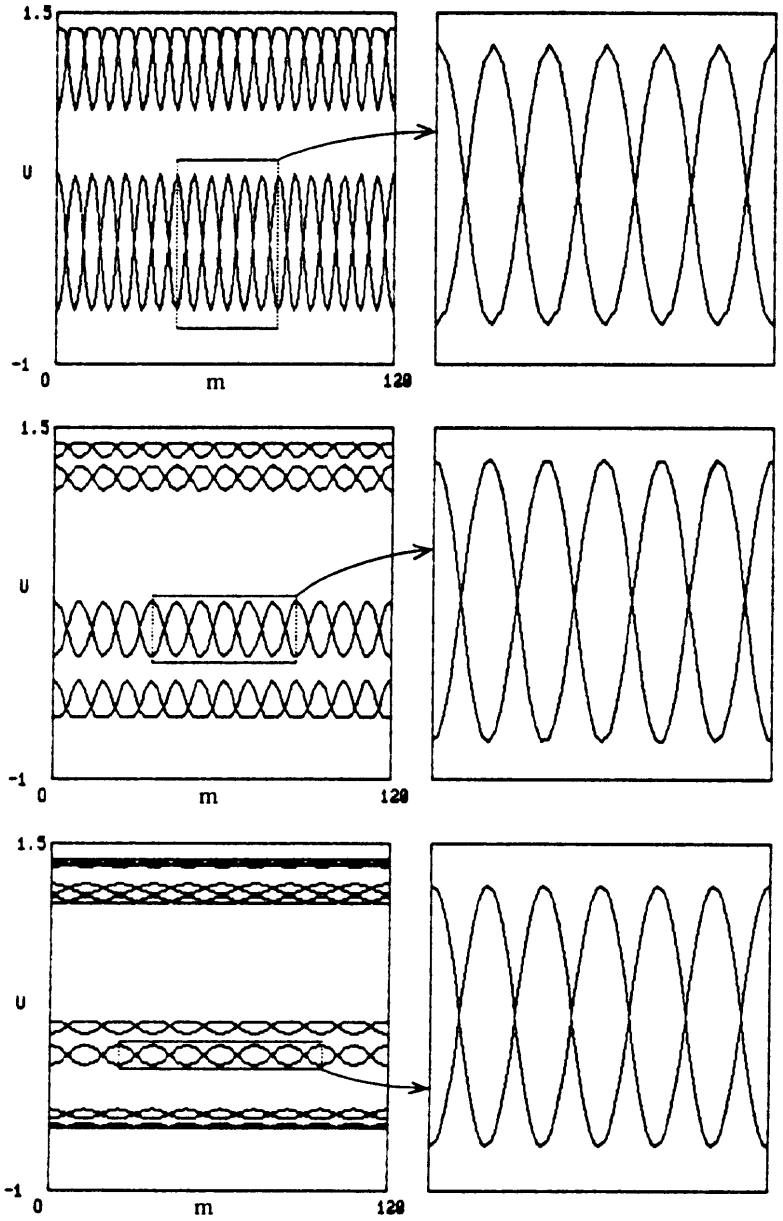

Figure 2.20 Space–amplitude diagrams illustrating scaling in the lattice model (2.36) with periodic boundary conditions. The values of parameters are $\lambda = 1.3$, $\gamma = -1.6$; $\lambda = 1.37949$, $\gamma = 1.27851$; $\lambda = 1.39652$, $\gamma = -1.02162$. The right-hand pictures show the parts inside the marked rectangles.

general view of the patterns while the right-hand ones depict the parts inside the smaller rectangles. Note that the initial conditions were chosen to satisfy the scaling requirements too: the wavelength of small sinusoidal perturbations increased from case to case by approximately $\sqrt{2}$.

2.5 Renormalization group and scaling in higher spatial dimensions

The generalization of the lattice RG analysis for higher spatial dimensions is straightforward. Suppose we have, for example, the two-dimensional square lattice with period-doubling system in each of the sites. As in Section 2.2, the fixed point of the lattice RG transformation is given by the system of uncoupled maps

$$\{\ldots g(u_{m,n})\ldots\}, \tag{2.38}$$

where m and n are the spatial indices. Restricting ourselves to the case of symmetrical coupling, let us assume that each site interacts with its four nearest neighbours in the same manner. The general asymptotic form of the perturbation of the fixed point is agains constructed with the aid of the universal functions Φ_0, Φ_1 and Φ_2. Thus, we may write in the linear approximation for the evolution operator through 2^k time steps:

$$\begin{aligned} u_{l+2k,m,n} &= g(u_{l,m,n}) + \Lambda\delta^k\Phi_0(u_{l,m}) \\ &+ Ca^k[\Phi_1(u_{l,m,n}, u_{l,m+1,n} + \Phi_1(u_{l,m,n}, u_{l,m-1,n}) \\ &+ \Phi_1(u_{l,m,n}\, u_{l,m,n+1}) + \Phi_1(u_{l,m,n}, u_{l,m,n-1})] \\ &+ D2^k[\Phi_2(u_{l,m,n}, u_{l,m+1,n} + \Phi_2(u_{l,m,n}, u_{l,m-1,n}) \\ &+ \Phi_2(u_{l,m,n}, u_{l,m,n+1}) + \Phi_2(u_{i,m,n}, u_{l,m,n-1})], \end{aligned} \tag{2.39}$$

where Λ, C and D are three essential parameters. Their interpretation and scaling properties are the same as in the one-dimensional case.

For computer illustration of the lattice scaling we turn to a phenomenon of frozen domain structures that exists in the two-dimensional lattices with diffusive coupling due solely to the presence of spatial discretization [8, 35, 36]. We take the evolution equation of the lattice in the form [8, 35]:

$$\begin{aligned} u_{l+1,m,n} &= 1 - \lambda u_{l,m,n}^2 \\ &- \left(\varepsilon\frac{\lambda}{4}\right)(u_{l,m+1,n}^2 + u_{l,m-1,n}^2 + u_{l,m,n+1}^2 + u_{l,m,n-1}^2 - 4u_{l,m,n}^2), \end{aligned} \tag{2.40}$$

with boundary conditions of periodicity

$$u_{l,0,n} = u_{l,M,n},\ u_{l,m,0} = u_{l,m,N}.$$

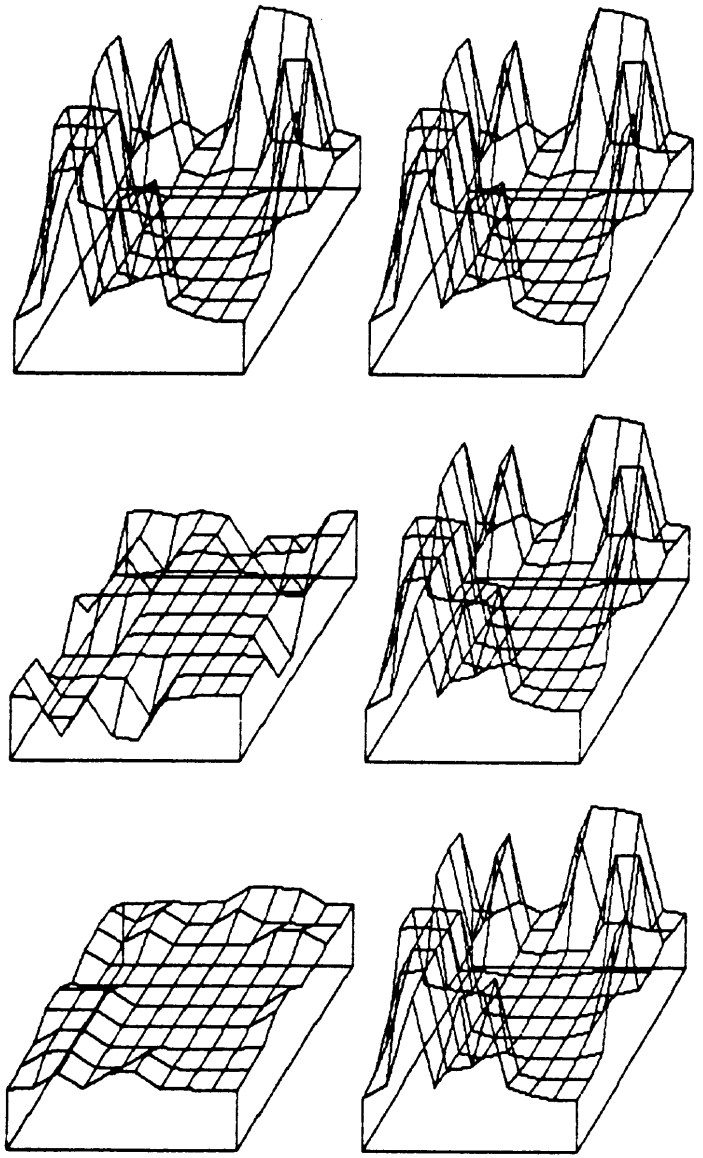

Figure 2.21 Illustrating of lattice scaling for sustained domain structures in two-dimensional lattice model with pure diffusive coupling (2.40). The lattice has size 10×10 and the periodic boundary conditions are used. The left-hand pictures show the instant spatial configurations repeating at each 2^k time step ($k = 1, 2, 3$). The right-hand pictures reproduce them but with the scaling variable ua^n plotted along the vertical axis. The parameters are $\lambda = 1.1$, $\varepsilon = 0.1$; $\lambda = 1.33666$, $\varepsilon = 0.05$; $\lambda = 1.38734$, $\varepsilon = 0.025$.

The upper left-hand picture in Figure 2.21 shows the spatial pattern arising from random initial conditions for some moment of time after completion of transients in the lattice of size 10×10 for coupling parameter $\varepsilon = 0.1$. This configuration is the period-2 fixed point of equation (2.40). One- and two-fold renormalization of parameters and dynamical variable using the scaling rule $\lambda \to \lambda_0 + (\lambda - \lambda_0)/\delta$, $\varepsilon \to \varepsilon/2$, $u \to u/\alpha$ gives the spatial configurations corresponding to period-4 and period-8 fixed points. These are shown in the next two left-hand pictures after some number of iterations other than the transients. In the right-hand column the same spatial patterns are reproduced with renormalization of the vertical axis scale by a. The good match is evident.

As in the one-dimensional case, multiple iterations of the RG transformation justify proceeding to the continuum limit. (The argument of the onset of Section 2.2.3 is also valid for higher spatial dimensions.) The diffusion term will contain the combination of derivatives $D(\partial^2/\partial x^2 + \partial^2/\partial y^2)$. So, the renormalization of D by 2 is equivalent to rescaling of the spatial variables by $\sqrt{2}$. Thus, the RG equation (2.23) and (2.24) remain valid, but all operators must be considered as acting on functions of two arguments $u(x, y)$. In particular, $\hat{S}u(x, y) = au(x\sqrt{2}, y\sqrt{2})$.

Furthermore, we may demonstrate the existence of limit operator G numerically. To this end the concrete model of the diffusive coupled lattice (2.40) may be taken for critical value λ_0 as the definition of the initial operator G_0. Let us take the initial probe functions in the form

$$u(x, y) = \sum A_{ij} \cos[(2\pi i/M)x + \varphi_i] \cos[(2\pi j/M)y + \psi_j],$$

where $A_{ij}, \varphi_i, \psi_j$ are random amplitudes and phases. Then, we may find numerically and compare the results of the action of the operators $G_n = \hat{S}^n G_0 \hat{S}^{-n}$ on the probe function for different values of n. Note that the selected values of M satisfy the relation $M \approx M_0 \cdot 2^{n/2}$. Figure 2.22 shows the computation data for two probe functions. It may be seen that the superposed data for $n = 3, 4, 5$ coincide very well. (The agreement become even more exact for larger n but the addition of the data to the plot would make it illegible.) The universality may be varified in the similar manner too: any model of the form (2.25) defined on the two-dimensional lattice or on a continuous two-dimensional medium leads in the critical situation to the same (up to normalization) operator G. This is true if the initial operator G satisfies conditions of translation invariance, symmetry, normalization, locality and dissipativity.

The spectrum of eigenvalues for the linearized fixed-point operator G may be analysed in the same way as in the one-dimensional case for the symmetric coupling. There are two essential eigenvectors. The first one has eigenvalue δ and is responsible for removing the control parameter from the critical point. The second one arises from the perturbation given in (2.39) by the term

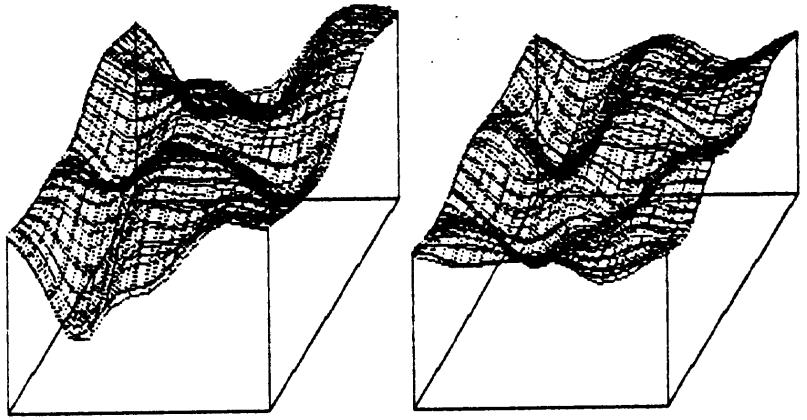

(a) (b)

Figure 2.22 Numerical verification of the existence of the fixed-point operator G for two-dimensional lattice with diffusive coupling for the critical value of the control parameter λ. The results of 8, 16 and 32 iterations of (2.40) are presented in renormalized form (see text) for two probe initial functions. The numbers of sites are 14×14, 20×20 and 28×28; the coupling constant is $\varepsilon = 0.4$.

proportional to C. It has the eigenvalue $a/2$ and is responsible for the inertial coupling.

To demonstrate the continuous scaling consider domain collapse in the two-dimensional diffusive coupled map lattice. It takes place for systems of two of more dimensions instead of the frozen domain behaviour in the one-dimensional systems [8, 35, 36]. The effect is suitable here for the illustration of continuum-limit behaviour because it is specific to the large coupling parameters $\varepsilon \geqslant 0.35$.

According to the scaling property, the domain of $(k+1)$th order would require twice the time interval for its destruction as compared with the domain of kth order if the ratio of their initial sizes is $\sqrt{2}$ and the ratio of deflections for λ from the critical value is $1/\delta$.

The evolutions of domains of 2nd and 3rd order may be compared as shown in Figure 2.23. The lattices (2.40) are taken of size 20×20 and 28×28 with ratio approximately $\sqrt{2}$. The initial conditions cause the appearance of the circular-form domain of the required order :

$$u_{0,m,n} = \begin{cases} u_0 \text{ for } (m - M/2)^2 + (n - M/2)^2 \leqslant M^2/9, \\ u_{2^{k-1}} \text{ for } (m - M/2)^2 + (n - M/2)^2 > M^2/9, \end{cases}$$

where u_0 and $u_{2^{k-1}}$ are the elements of the period-2^k cycle of the local map with $k = 2$ and 3. The spatial configurations are shown in Figure 2.23 realized

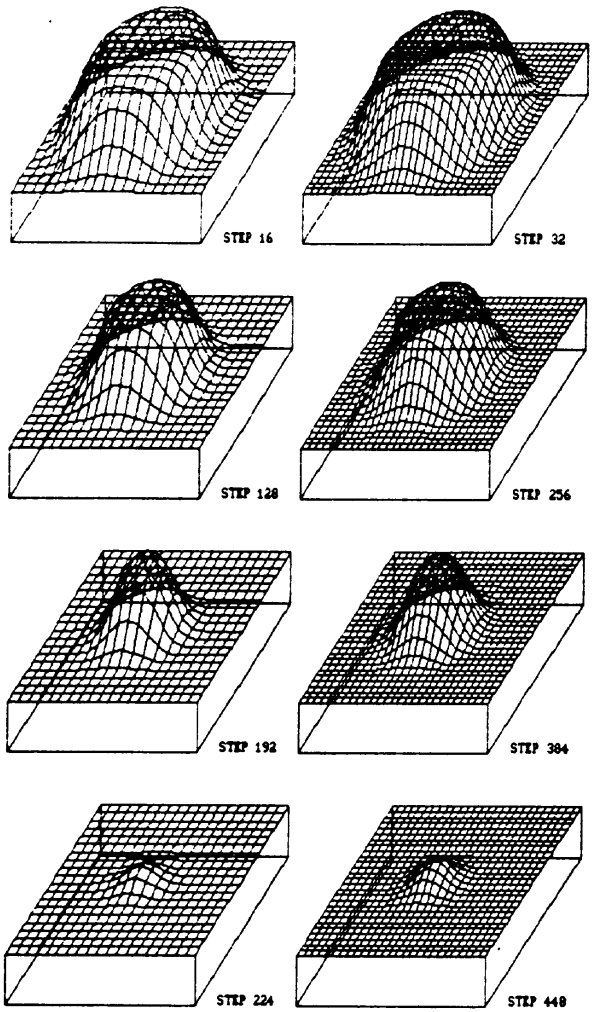

Figure 2.23 Illustration of continuous scaling in the two-dimensional lattice model with diffusion (2.40), $\varepsilon = 0.4$. The left- and right-hand columns show consecutive spatial configurations for two cases under initial conditions causing the formation of circle domains of 2nd and 3rd order. For the left-hand pictures $\lambda = 1.31$, size is 20×10. For the right-hand $\lambda = 1.38163$, size is 28×28. The scaling variable is plotted along the vertical axis.

at several sequential time steps. The scaling variable ua^{k-1} is plotted along the vertical axis. We can see the developing process of destruction of the domains with good agreement of the left-hand and right-hand pictures according to the expected scaling.

Another illustration of continuous scaling in the two-dimensional system was presented in [25]. The authors demonstrated the scaling behaviour of threshold geometric size from which the Lyapunov exponent of the chaotic spatiotemporal dynamics becomes approximately the same as for the large system: this size increases by $\sqrt{2}$ under decreasing of $\lambda - \lambda_0$ by δ.

2.6 Conclusion

In conclusion we shall briefly consider the achievements, disadvantages and properties of the RG approach to CML.

Thanks to RG analysis, the universality classes represented by CML are revealed. This allows us to find the full system of CML models for spatiotemporal dynamics close to the onset of chaos. The concept of scaling gives a powerful tool for organizing the classifying a variety of results from empirical computer investigations into CML dynamics.

There are some disadvantages intrinsic to this approach as compared with the classical Feigenbaum analysis of period-doubling in one-dimensional maps. One is the larger number of essential parameters and a second is the severe requirement of translation invariance, which is natural in some real-life systems, but not in others. Thirdly, not all of the realizable states are acceptable for RG consideration even at the critical point, in contrast to the simple period-doubling systems.

In spite of these observations I believe that the information given by RG analysis for the spatially extended system is invaluable and this point of view is supported by the results discussed above.

As for possible directions of further investigations using the RG approach, we may mention the application of CMLs for the description of real systems dynamics using the universality, the development of the formalism for other types of local dynamics, more detailed consideration of phenomena in higher spatial dimensions, and the rigorous mathematical foundation of the RG approach.

References

[1] M. J. Feigenbaum, Quantitative universality for a class of nonlinear transformations, *J. Stat. Phys.* **19** (1978), no 1, 25–32.

[2] M. J. Feigenbaum, The universal metric properties of non-linear transformations, *J. Stat. Phys.* **21** (1979), no 6, 669–706.

[3] B. Hu and J. Rudnik, Exact solution to the Feigenbaum renormalization group equation for intermittency, *Phys. Rev. Lett.* **48** (1982), no 24, 1645–8.

[4] R. Oslund, D. Rand, J. Sethna and E. Siggia, Universal properties of the transition from quasiperiodicity to chaos in dissipative systems, *Physica* **D8** (1983), 303–42.

[5] K. Kaneko, Period doubling of kink-antiking patterns, quasiperiodicity in antiferrolike structures in coupled logistic lattice, *Progr. Theor. Phys.* **72** (1984), no. 3, 480–6.

[6] K. Kaneko, Spatial period-doubling in open flow, *Phys. Lett.* **A111** (1985), no 8, 321–5.
[7] J. P. Crutchfield and K. Kaneko, Phenomenology of spatio-temporal chaos, in *Directions in Chaos*, (ed. Hao Bai-lin, World Scientific, Singapore, 1987), 272–353.
[8] K. Kaneko, Simulating physics with coupled map lattices, in *Formation, Dynamics and Statistics of Patterns* (ed. K. Kaneko *et at.*, World Scientific, Singapore, 1990).
[9] I. Waller and R. Kapral, Spatial and temporal structure in systems of coupled nonlinear oscillators, *Phys. Rev.* **A30** (1984), no 4, 2047–55.
[10] S. P. Kuznetsov and A. S. Pikovsky, Universality and scaling of period-doubling bifurcations in a dissipative distributed medium, *Physica* **D19** (1986), no 3, 384–96.
[11] J. D. Keeler and J. D. Farmer, Robust space-time intermittency and 1/f noise, *Physica* **D23** (1986), 413.
[12] H. Chaté and P. Manneville, Criticality in cellular automata, *Physica* **D45** (1990), no 1–3, 122–35.
[13] S. P. Kuznetsov, Universality and scaling in behavior of coupled Feigenbaum systems, *Izv. VUZov—Radiofizika* **T. 28** (1985), no 8, 991–1007. (Translations: *Radiophysics and Quantum Electronics* **28**, 681–95.
[14] S. P. Kuznetsov, Scale-invariant structure of parameter space for coupled Feigenbaum systems, *J. Technich. Fiz.* **55** (1985), no 9, 1830–4 (in Russian).
[15] S. P. Kuznetsov and A. S. Pikovsky, Interaction of systems with stochastic behavior, in *Nonlinear Waves. Structures and Bifurcations* (Nauka, Moscow, 1987), 237–51 (in Russian).
[16] A. S. Pikovsky and V. G. Shekhov, Universal behavior of a coupled circle map, in *Nonlinear World. Proc. IV Int. Workshop on Nonlinear and Turbulent Processes in Physics* (Naukova Dumka, Kiev, 1989), Vol. 2, 406–8.
[17] S. P. Kuznetsov, On critical behavior of one-dimensional lattices, *Pis'ma J. Technich. Fiz.* **9** (1983), no 2, 94–8 (in Russian).
[18] S. P. Kuznetsov, On model description of coupled dynamical systems near the transition point order–disorder, *Izv. VUZov–Fizika* **27** (1984), no 6, 87–96 (in Russian).
[19] H. Kook, F. H. Ling and G. Schmidt, Universal behavior of coupled nonlinear systems, *Phys. Rev.* **A43** (1991), no 6, 2700–8.
[20] R. Kapral, Pattern formation in two-dimensional arrays of coupled discrete time oscillators, *Phys. Rev.* **A31** (1985), no 6, 3868–79.
[21] S. P. Kuznetsov, Period-doubling bifurcations in a simple model of expanded system, *Izv. VUZov—Radiofizika* **25** (1982), no 11, 1364–8 (in Russian).
[22] A. P. Kuznetsov, S. P. Kuznetsov and I. R. Sataev, Scaling properties of spatio-temporal dynamics in period doubling coupled map lattices, in *Nonlinear World. Proc. IV Int. Workshop on Nonlinear and Turbulent Processes in Physics* (Naukova Dumka, Kiev, 1989), Vol. 2, 383–6.
[23] S. P. Kuznetsov, Renormalization group, universality and scaling in dynamics of one-dimensional auto-wave media, *Izv. VUZov—Radiofizika* **29** (1986), no 8, 888–902. (Translation : *Radiophysics and Quantum Electronics* **29**, 679–92.)
[24] F. Kaspar and H. Shuster, Scaling at the onset of spatial disorder in coupled piecewise linear maps, *Phys. Lett.* **A113** (1986), no 9, 451–3.
[25] T. Bohr and O. B. Christensen, Size dependence, coherence, and scaling in turbulent coupled-map lattices, *Phys. Rev. Lett* **63** (1989), no 20, 2161–4.
[26] I. S. Aranson, A. V. Gaponov-Grekhov and M. I. Rabinovich, The onset and spatial development of turbulence in flow systems, *Physica* **D33** (1988), 1–20.

[27] B. P. Bezruchko, Yu. V. Gulyaev, S. P. Kuznetsov and E. P. Seleznev, New type. of critical behavior of coupled systems at onset of chaos, *Doklady Acad. Nauk SSSR* **287** (1986), no 3, 619–22. (Translations: *Sov. Phys. Dokl.* **31**, 258–60.)
[28] S. P. Kuznetsov, Dynamics of two unidirectionally coupled Feigenbaum systems near onset of hyperchaos. Renormalization group analysis, *Izv. VUZov—Radiofizika* **33** (1990), no 7, 788–92 (in Russian).
[29] K. Kaneko, Pattern dynamics in spatiotemporal chaos. Pattern selection, diffusion of defect and pattern competition intermittency, *Physica* **D34** (1989), no 1–2, 1–42.
[30] K. Kaneko, Transition from torus to chaos accompanied by frequency locking with symmetry breaking. In connection with the coupled logistic map, *Progr. Theor. Phys.* **69** (1983), no 5, 1427–42.
[31] J. Froyland, Some symmetric two-dimensional dissipative maps, *Physica* **D8** (1983) 423–34.
[32] Yuan Jian-min, Tung-Mingwhei, Feng Da Hsaan and L. Narducci, Instability and irregular behavior of coupled logistic equations, *Phys. Rev.* **A28** (1983), no 3, 1662–6.
[33] T. Hogg and B. A. Huberman, Generic behavior of coupled oscillators, *Phys. Rev* **A29** (1984) no 1, 275–81.
[34] H. Fujisaka and T. Yamada, A new intermittency in coupled dynamical systems, *Progr. Theor. Phys.* **74** (1985), no 4, 917–21.
[35] K. Kaneko, Spatiotemporal chaos in one- and two-dimensional coupled map lattices, *Physica* **D37** (1989), 60–82.
[36] J.-L. Oppo and R. Kapral, Discrete models for the formation and evolution of spatial structure in dissipative systems, *Phys. Rev.* **A33** (1986), no 6, 4219–31.